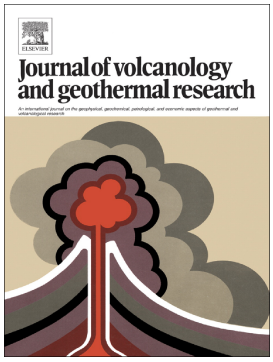

Trace element transport by volcanic gases at Vulcano (Sicily, Italy) – Speciation, deposition and fluxes

Celine L. Mandon, Hanna Kaasalainen, Sergio Calabrese, Everett L. Shock, Panjai Prapaipong, Franco Tassi, Ingvi Gunnarsson, Jóhann Gunnarsson-Robin, Andri Stefánsson

PII: S0377-0273(24)00228-2

DOI: https://doi.org/10.1016/j.jvolgeores.2024.108235

Reference: VOLGEO 108235

To appear in: *Journal of Volcanology and Geothermal Research*

Received date: 15 June 2024

Revised date: 1 November 2024

Accepted date: 11 November 2024

Please cite this article as: C.L. Mandon, H. Kaasalainen, S. Calabrese, et al., Trace element transport by volcanic gases at Vulcano (Sicily, Italy) – Speciation, deposition and fluxes, *Journal of Volcanology and Geothermal Research* (2024), https://doi.org/10.1016/j.jvolgeores.2024.108235

Trace element transport by volcanic gases at Vulcano (Sicily, Italy) – speciation, deposition and fluxes

Celine L. Mandon[1]*, Hanna Kaasalainen[2], Sergio Calabrese[3,4], Everett L. Shock[5,6], Panjai Prapaipong[5], Franco Tassi[7], Ingvi Gunnarsson[8], Jóhann Gunnarsson-Robin[1], Andri Stefánsson[1]

[1] Nordic Volcanological Center, Institute of Earth Sciences, University of Iceland, Sturlugata 7, Reykjavik 102, Iceland
[2] Geological Survey of Finland, Vuorimiehentie 5, P.O. Box 96, FI-02151, Espoo, Finland
[3] Dipartimento di Scienze della Terra e del Mare (DiSTeM), Università di Palermo, Palermo, Italy.
[4] Istituto Nazionale di Geofisica e Vulcanologia, Sezione di Palermo, Palermo, Italy
[5] School of Earth and Space Exploration, Arizona State University, Tempe, AZ, USA
[6] School of Molecular Sciences, Arizona State University, Tempe, AZ, USA
[7] Department of Earth Sciences, University of Florence, via La Pira 4, Firenze 50121, Italy
[8] Reykjavík Energy, Bæjarháls 1, 110 Reykjavík, Iceland
* corresponding author: celine@hi.is; ORCID# 0000-0002-7671-0995

Abstract

The geochemistry of trace elements in volcanic gas emissions at Vulcano (Sicily, Italy) was investigated. Trace element concentrations in 94-412°C fumarole gases span over 10 orders of magnitude, from ~0.01 pmol/mol to ~300 µmol/mol, with some metalloids (B, Si) being the most abundant, followed by alkali, alkaline earth, and certain transition metals, and rare earth elements typically displaying the lowest concentrations. Thermodynamic modeling predicts most trace elements to be transported as chloride, hydroxide, and mixed hydroxy-chloro gas species (LiCl, KCl, NaCl, RbCl and CsCl, $Be(OH)_2$, $Mg(OH)_2$, $MgCl_2$, $CaCl_2$, $SrCl_2$, CaCl(OH), $TiOCl_2$, VOCl, $VOCl_2$, $VOCl_3$, $NbOCl_3$, $Cr(OH)_3$, $CrCl_3$, $Fe(OH)_2$, $FeCl_2$ $Co(OH)_2$, $CoCl_2$, $Ni(OH)_2$ to $NiCl_2$, $Cd(OH)_2$, $CdCl_2$, $Re(OH)_3$, $ReCl_3$, $ZnCl_2$, AgCl, $WO_2(OH)_2$, $Al(OH)_3$, $Si(OH)_4$, $B(OH)_4$, TlO, $GaCl_3$, SbCl, $MnCl_2$, CuCl). Sulfide, hydrate, and elemental gas species are also important for some elements (Cd, AuS, Hg, PbS_2, BiS, Bi, AsS, As_2S_3, TeS, SeH, SeS). However, for many trace elements, speciation remains uncertain or unknown due to a lack of thermodynamic data. Upon cooling and decompression of the volcanic gas, most trace elements are predicted to reach gas-solid equilibrium, resulting in the formation of secondary minerals. At high temperatures (~700-1000°C), the mineral assemblage forming is dominated by quartz, Ca-Na-K feldspars, and Mg-pyroxene, containing minor concentrations of other alkali and alkaline earth metals. Further cooling and decompression leads to the formation of minerals including magnetite, pyrite, chalcocite, and chalcopyrite together with other less abundant oxides (V, Cr, Ga, W, and Sn) and sulfides (Zn, Pb, Ni, Co, Cd, Mo, Ag, As, and Bi), and eventually a range of sulfates and sulfosalts (Li, K, Na, Rb, Cs, Be, Mg, Ca, Sr, Bi, Mn, Fe, Zn, Pb, and Sn) at the lowest temperatures (~100-300°C). For most trace elements, fumarole emission concentrations reflect higher gas-solid equilibrium temperatures than those observed during sampling, suggesting gas-solid equilibria at high temperatures followed by incomplete re-equilibration upon further cooling near the surface.

Trace element fluxes span over eight orders of magnitude, ranging from >100 kg/day to ~$1 \cdot 10^{-6}$ kg/day. Silica, Al, and B consistently exhibit the highest fluxes, followed by alkali and alkaline earth metals, various transition metals and metalloids, with rare earth elements and actinides displaying the lowest fluxes. Generally, the trace element fluxes are lower compared to neighboring Stromboli and Etna, except for Pb, Bi, B, As, Sb, and Te.

Keywords: Volcanic gas; trace elements; gas speciation; thermodynamic modeling

1. Introduction

Volcanic gas emissions constitute significant sources of many elements to the atmosphere, including volatile metals, metalloids, and aerosols (Nriagu, 1989, Hinkley et al., 1999, Mather et al., 2003). Additionally, the composition of volcanic gases offers valuable insights into volatile element emissions into overlying hydrothermal systems and the formation of porphyry and epithermal ore deposits. The volatile element melt composition, together with pressure (depth), temperature, and the degree of crystallization of the degassing magma, govern the composition of the source magmatic gas (e.g., Nash and Crecraft, 1985, Blundy and Wood, 2003, Mather et al., 2012, Iveson et al., 2019). Moreover, as volcanic gases rise to the surface, their chemical composition may undergo changes through a number of processes, including interactions with the host rock and/or hydrothermal system (Symonds et al., 2001, Henley and Seward, 2018, Henley and Fischer, 2021), cooling, decompression, and oxidation upon mixing with the atmosphere. These processes, for example, result in mineral deposition, as evident from incrustations around fumarolic vents and the formation of aerosols in the atmosphere (e.g., Stoiber and Rose, 1974, Allen et al., 2000, Africano et al., 2002, Gauthier et al., 2016, Mandon et al., 2019, Inostroza et al., 2020, Ilyinskaya et al., 2021).

Data on the major element composition of volcanic gas are readily available today, both based on direct measurements of volcanic gas and passive fumarole emissions. High-temperature volcanic gas is typically dominated by H_2O (~70-95 mol%), followed by CO_2 (~1-15 mol%) and SO_2 (<1-15 mol%), with lesser amounts of HCl, HF, HBr, CO, H_2S, and H_2 (e.g., Symonds et al., 1994, Delmelle et al., 2000, Bobrowski et al., 2003). However, available data on the trace element composition of volcanic gas are limited. Data are available for volcanic eruption plumes from various geological settings like Etna and Stromboli (Italy), Ambrym (Vanuatu), Holuhraun (Iceland), Kilauea (Hawaii, USA), Erta Ale (Ethiopia), Tolbachik (Russia) (Aiuppa, 1999, Allard et al., 2000, Calabrese et al., 2011, Zelenski et al., 2013, Zelenski et al., 2014, Gauthier et al., 2016, Mason et al., 2021), and degassing volcanic hydrothermal systems, for example, Kudriavy (Russia), Merapi (Indonesia), Augustine (USA), Usu and Satsuma-Iwo Jima (Japan), Cerro Negro, Momotombo and San Cristobal (Nicaragua), Poas (Costa Rica), and Iceland (Gemmell, 1987, Symonds et al., 1987, Symonds et al., 1992, Hedenquist et al., 1994, Taran et al., 1995, Symonds et al., 1996, Wahrenberger et al., 2002, Kaasalainen and Stefánsson, 2012). Based on these studies, the trace element composition, including metal and metalloid concentrations, varies over ten orders of magnitude from $<10^{-12}$ to >0.01 mol%.

Our understanding of trace element concentrations and transport by volcanic gases relies on several factors. Sampling of volcanic gas at extremely high temperatures is difficult as well as chemical analysis of trace elements in samples containing high levels of S, Cl and F. Moreover, the chemical composition of samples from natural manifestations may change from source to surface due to various factors, including gas-rock interaction, gas condensation and interaction with shallow overlying hydrothermal fluids. Equilibrium thermodynamic calculations have been applied to model such trace element transport behavior (Symonds et al., 1987, Quisefit et al., 1989, Symonds et al., 1992, Symonds and Reed, 1993, Getahun et al., 1996, Wahrenberger et al., 2002, Henley and Seward, 2018, Mandon et al., 2020). The results indicate that most metals and metalloids interact with major gases to form chlorine, sulfur and hydrated gaseous compounds (e.g., Henley and Seward, 2018). However, the outcome of such calculations is dependent on the quality of the thermodynamic data and thermodynamic equations used, neither being well

defined at these high temperatures and moderate to low pressures (e.g., Pokrovski et al., 2013, Henley and Seward, 2018). Alternatively, trace element behavior has been interpreted qualitatively by comparing results from different geological settings. For instance, variations in halogen concentrations have been employed to elucidate differences in trace element emissions between arc and intraplate volcanoes, including notably high emissions from certain halogen-rich intraplate volcanoes (Gauthier et al., 2016, Mandon et al., 2019, Mason et al., 2021, Zelenski et al., 2021).

The aim of this study is to enhance our understanding of the abundances and transport characteristics of trace elements within volcanic gases. We intend to link measured trace abundances in fumarolic fields along with composition and spatial distribution of mineral deposits observed at extinct volcanoes to processes occurring during magmatic gas transport from source to surface, focusing on the influence of major gas composition, cooling and decompression on speciation and mineral precipitation. For this, fumarole emissions from Vulcano Island (Italy) were collected using various methods to assess the reproducibility and accuracy of the sampling and analytical techniques. Trace element abundances were obtained for a range of fumarole temperatures and compositions between 2008 and 2022. Additionally, we employed thermodynamic modeling to analyze gas speciation and gas-solid interactions as the gases rise from depth after exsolution from a magma to the fumarole where they are emitted. We compared these models with data on gas composition and solid sublimates to gain insight into the factors controlling trace element concentrations and transport behavior.

2. Study area

Vulcano Island (Italy) forms part of the Aeolian volcanic arc. Its eruptive and subsurface materials include basalt, trachyte, and rhyolite (Clocchiatti et al., 1994, Zanon et al., 2003, Peccerillo et al., 2006, De Astis et al., 2013, Costa et al., 2020). The youngest edifice on Vulcano is La Fossa (~5.5 kyrs), hosts a fumarolic field (Fig. 1) (De Astis et al., 2013). Gas emissions mainly consist of H_2O (>80 mol%), CO_2 (4-20 mol%), sulfur volatiles (SO_2 and H_2S; 0.1-1.5 mol%), and HCl (0.02-0.8 mol%), along with lower concentrations of HF, H_2, N_2, and He (Chiodini et al., 1993, Nuccio et al., 1999, Paonita et al., 2002, Paonita et al., 2013). A hydrothermal system, partially fed by seawater, is the main source of thermal manifestations at the base of the La Fossa cone (Capasso et al., 1992, Nuccio et al., 1999, Paonita et al., 2002, Federico et al., 2010).

Studies conducted over the past few decades have observed variations in fumarolic gases during periods of unrest, characterized by increased gas temperature and fluxes and changes in gas composition (increasing CO_2, He and N_2 concentrations relative to H_2O), followed by intermittent periods of repose (Martini et al., 1980, Carapezza et al., 1981, Cioni and D'Amore, 1984, Badalamenti et al., 1991, Barberi et al., 1991, Chiodini et al., 1993, Chiodini et al., 1995, Capasso et al., 1997, Italiano et al., 1998, Capasso et al., 1999, Nuccio et al., 1999, Paonita et al., 2002, Paonita et al., 2013, Inguaggiato et al., 2022). The most recent unrest episode occurred between 2021 and 2022 (Aiuppa et al., 2022, Federico et al., 2023). These fluctuations in gas composition during unrest and repose periods are attributed to variations in the mixing ratio between magmatic (enriched in CO_2, He and N_2) and hydrothermal gases possibly related to magma injections in the deep chamber (Chiodini et al., 1992, Chiodini et al., 1993, Chiodini et al., 1995, Aiuppa et al., 2005, Granieri et al., 2006, Taran, 2011, Aiuppa et al., 2022).

Elevated concentrations of metals and metalloids have been observed in air particulates near the volcano (Dongarrà and Varrica, 1998, Varrica et al., 2000, Fulignati et al., 2006). Furthermore, metal and metalloid-rich sublimates and incrustations are common at the La Fossa fumarole field, including sulfur, salammoniac, sassolite, sulfides, and sulfosalts (e.g. Garavelli et al., 1997, Fulignati and Sbrana, 1998, Vurro et al., 1999, Garavelli et al., 2005, Demartin et al., 2009, Pinto et al., 2014). Additionally, studies of hydrothermal waters have shown elevated metal concentrations relative to source water, partly influenced by magmatic gas input (Brondi and Dall'Aglio, 1991, Aiuppa et al., 2000, Falcone et al., 2022). Nevertheless, the trace element concentrations in volcanic gas emissions at Vulcano remain poorly characterized (Cheynet et al., 2000).

3. Methods

3.1. Sampling and analytical methods

Volcanic gas samples of fumarole emissions were collected during four sampling campaigns in 2008, 2009, 2012 and 2022 (Fig. 1). The first three sampling campaigns took place during periods of repose, while the last one was during the unrest. For sampling, a ~50-cm long Pyrex glass or titanium tube was inserted into the fumarole and connected to the sampling bottles using a silicon tube. Samples for major elemental determination (H_2O, CO_2, CH_4, SO_2, H_2S, H_2, O_2, N_2, Ar, Cl, and F) were collected into pre-evacuated ~50-100 ml gas-bulbs containing 4M NaOH (ACS reagent) or 50% KOH (ACS reagent) (~30 ml per 100 ml) solution with and without 1M Zn-acetate or 0.15M $Cd(HO)_2$ for SO_2 and total sulfur (S_{tot}) analysis, respectively. All analysis were conducted at the University of Iceland if not otherwise indicated. Non-condensable gases (CH_4, H_2, O_2, N_2 and Ar) were determined by gas chromatography (GC). The concentration of other major elements was analyzed in the condensate. The CO_2 was analyzed by titration (Arnórsson et al., 2006), the Cl and F concentrations by ion chromatography (IC) and S_{tot} as SO_4 by ion chromatography on samples that had previously been oxidized using H_2O_2 (30% Suprapur®) and UV-light. The concentration of SO_2 was analyzed in samples containing Zn-acetate. In the sample bottle, H_2S was assumed to quantitatively precipitate as $ZnS_{(s)}$, and subsequently the precipitate was filtered off. The SO_2 was further oxidized to completion using H_2O_2 and UV-light and analyzed using ion chromatography as SO_4. The concentration of H_2S was then calculated as the difference between S_{tot} and SO_2.

Three sampling methods were applied for trace element determination (Ag, Al, As, Au, B, Ba, Be, Bi, Ca, Cd, Ce, Co, Cr, Cs, Cu, Dy, Er, Eu, Fe, Ga, Gd, Ge, Hf, Hg, Ho, Ir, K, La, Li, Lu, Mg, Mn, Mo, Nb, Nd, Ni, P, Pb, Pd, Pr, Pt, Rb, Re, Rh, Ru, Sb, Sc, Se, Si, Sm, Sn, Sr, Ta, Tb, Te, Th, Ti, Tl, Tm, U, W, V, Y, Yb, Zn, Zr). Firstly, direct vapor condensate samples were collected into Teflon bottles, these filtered through 0.2 µm filter (cellulose acetate or Teflon) on-site, diluted with deionized water and acidified with trace element grade 67% HNO_3 (1 mL per 100 mL solution). Condensates collected in 2022 were not treated immediately after collection, but filtered and acidified weeks after sampling. Secondly, samples were collected into pre-evacuated gas bottles containing 25% NH_4OH (Merck Suprapur®) (Sortino et al., 2006) solution (~30 mL per 100 mL bottle), followed by dilution with deionized water. Thirdly, samples were collected in three condensers in line, with the last two containing 0.3M NaOCl solution for efficient dissolution and oxidation of volatile elements. A steady gas flow (0.2-0.3 mL/min) through the traps was maintained by an air-pump at the end of the line. The condensate sample

was filtered, diluted, and acidified as previously described whereas the NaOCl containing sample was not further treated. Following analysis, the concentrations of the gas emissions were added from various traps and normalized to the vapor condensate collected. By filtering condensate samples on site, we assumed any solid particles > 0.2 µm diameter (both host rock particles from magma fragmentation or conduit erosion and particles formed by direct condensation of the magmatic gas phase) to be removed from solution, the trace element content reflecting that of gaseous molecules solely.

The trace element concentrations were analyzed as follows: with a single-collector double-focusing magnetic sector inductively coupled plasma mass spectrometer (Thermo Finnigan Element-2) at Arizona State University for the 2008 and 2009 datasets, using the most appropriate resolution for each element; an inductively coupled plasma sector field mass spectrometer at ALS Scandinavia accredited commercial laboratory for the 2012 dataset using screening analysis; a single-quadrupole inductively coupled plasma mass spectrometer (Thermo Fisher iCap™ RQ) at the University of Iceland for the 2022 dataset, run in collision cell mode (He). See Supplementary material for further details on the ICP-MS settings and operating conditions. All samples were run using multiple dilutions to prevent and overcome interferences due to high sulfur load and matrix effects. Detection limits (replicates of multi-element standard measurements with a 99% confidence level) and blank reagent concentrations were further determined for each type of sample matrix (Supplementary material). For individual elements, the trace analytical reproducibility was generally <10% at the 95% confidence level based on double to multiple analysis of each sample. The analytical accuracy based on standard solutions analysis (SPEX standards) were generally <3% and the analytical detections based on matrix matched standard solutions was <10 ppb for most elements but as high as ~4 ppm in some cases (Supplementary material). Some elements (Be, Zr, Nb, Ag, Cd, Hf, Ta, W, Re, Au, Tl, Bi, Ga, Ge, Se) had high uncertainties (>5-10% rsd) and should thus be regarded as qualitative. Rare Earth Elements and Platinum Group Elements results are indicative.

3.2.Thermodynamic modelling

Trace elements in volcanic gas can exist as gaseous compounds, liquids, and solid particles. To model this complex composition, equilibria among solids and gases were considered. The calculations were performed using HSC Chemistry 10 software (https://www.mogroup.com/portfolio/hsc-chemistry/), employing Gibbs energy minimization to determine the equilibrium composition of the system at specified temperature and pressure conditions.

The purpose of the thermodynamic modeling was to provide insight into the trace element gaseous speciation and the composition of the solid condensed phases which the gas is in equilibrium with over the temperature and pressure range of the ascending volcanic gas. For this purpose, the gas was allowed to cool and decompress from 1000°C and 1000 bar consistent with an initial lithostatic pressure of magma at ~4 km depth to surface at 100°C and 2 bar. The gas was assumed to rapidly decompress to just above atmospheric pressures (~3 bar) while cooling to the maximum fumarole temperatures of 650°C observed at Vulcano. Following this quasi isenthalpic expansion to shallow depth, conductive cooling occurs at near-constant pressure down to 2 bar. This pressure-temperature path used for thermodynamic modelling is detailed in Supplementary material.

For the calculations, a typical major gas composition was used, based on an enriched CO_2 sample (#FNB from 2022, Supplementary material), to represent the deep gas composition and minimize potential influence from hydrothermal fluids in the shallow part of the conduit. The H_2 content was adjusted to reflect high temperature conditions. In contrast, trace element concentrations for the calculations were averaged from all the samples analyzed. The input gas composition for the thermodynamic calculations is provided in the Supplementary material.
The HSC Chemistry 10 database served as the foundation for the calculations. This database incorporates available gaseous and mineral thermodynamic data from the literature, including Gibbs energy (ΔG), enthalpy (ΔH), entropy (S), and heat capacity (C_p) data. In some instances, data for certain gaseous species were extrapolated from low to high temperatures using the appropriate heat capacity function. Gas species were added in the input file as an ideal gas mixture, while solids were assumed to form pure phases. Initially, all gaseous species and minerals for selected components were included in the calculations but were subsequently narrowed down to include only those observed in significant concentrations ($>10^{-15}$ mol%). In total, 265 gaseous species and 214 minerals were eventually included in the calculations (Supplementary material).

4. Results

4.1 Major element composition

The volcanic gases emissions collected at Vulcano had temperatures between 94 and 412 °C (Table 1). The gas composition (n =22) was dominated by H_2O (82.3-93.6 mol %), followed by CO_2 (5.44-17.5 mol %), HCl (0.022-0.81 mol %), SO_2 (0.032-0.42 mol %), H_2S (0.010-0.26 mol%), N_2 ($8.0\cdot10^{-3}$-0.20 mol%), H_2 ($5.6\cdot10^{-3}$-0.17 mol%), CH_4 ($1.5\cdot10^{-5}$-0.065 mol%) and HF ($1.1\cdot10^{-3}$-0.050 mol%). Samples collected in 2022 displayed higher concentrations of CO_2 and lower HCl contents compared to samples collected during 2008-2012. Duplicate samples collected at the same time from the same fumarole display reasonably similar values with differences being: <1% for H_2O, <5-15% for CO_2, SO_2, HCl and HF and <25-30% for H_2, CH_4, N_2 and O_2 and <50% for H_2S.

4.2 Trace element composition

The concentrations of 64 trace elements were analyzed in 38 samples of volcanic gas emissions. Alkali metals (Li, Na, K, Rb, Cs) and alkaline earth metals (Be, Mg, Ca, Sr, Ba) exhibit concentrations ranging from 0.001 to 8588 nmol/mol (Table 1, Fig. 2). Among these, Na, K, Mg, and Ca are the most abundant, whereas Rb, Cs, and Be have comparatively lower concentrations. All concentrations exceed the analytical detection limit, indicating significant findings.

The concentrations of transition metals (Sc, Ti, V, Cr, Mn, Fe, Co, Ni, Cu, Zn, Zr, Nb, Mo, Ru, Rh, Pd, Ag, Cd, Hf, Ta, W, Re, Ir, Pt, Au, Hg) spanned 9 orders of magnitude, ranging from approximately 10^{-5} to 10^{4} nmol/mol. The most abundant elements were Fe, Ti, and Zn (1 – 18,825 nmol/mol), followed by Cr, Mn, Ni, and Cu (0.4 – 336 nmol/mol), and V, Mo, Ta, Cd, Co, Zr, Hf, Hg, W, and Nb (0.002 – 54 nmol/mol). For most transition metals (Sc, Ti, V, Cr, Mn, Fe, Co, Ni, Cu, Zn, Zr, Mo, Pd, Ag, Cd, Ta, W, Ir, and Hg), concentrations were above the analytical detection limit (Fig. 2), indicating significant results. However, for other transition

metals (Nb, Re, Ru, Rh, Hf, Pt, and Au), concentrations were just higher or similar to analytical detections, suggesting that results for those elements should be interpreted with caution.

The concentrations of post-transition metals (Al, Ga, Tl, Sn, Pb, Bi), metalloids (B, Si, Ge, As, Sb, Te), and non-metals (P, Se) also spanned a wide concentration range ($7 \cdot 10^{-4}$ – $3 \cdot 10^{5}$ nmol/mol). Boron and silicon emerged as the most abundant with consistently elevated concentrations (555 – 300755 nmol/mol), followed by Al, As, Pb, and P (0.1 – 140638 nmol/mol), Bi, Tl, Se, Sb, and Sn ($7 \cdot 10^{-4}$ – 623 nmol/mol), and Te, Ga, and Ge ($4 \cdot 10^{-3}$ – 18 nmol/mol). Most concentrations of the post-transition metals, metalloids, and non-metals were above the analytical detection limit, with some exceptions (Sn, P, and Se) suggesting that results for the latter elements should be interpreted with caution.

The concentration of rare earth elements and selected actinides (Y, La, Ce, Pr, Nd, Sm, Eu, Gd, Tb, Dy, Ho, Er, Tm, Yb, Lu, Th, U) were consistently low (10^{-5} - 2 nmol/mol), with many data points close to the analytical detection limits (La, Ce, Pr, Nd, Sm, Gd, Dy, Ho, Er, Tm, Yb, Lu, and Th).

5. Discussion

5.1. Volcanic gas compositions and data quality

Trace elemental concentrations in volcanic gas emissions are known to depend on the methods applied for sampling and analysis (e.g., Fischer et al., 1998b, Sortino et al., 2006, Zelenski et al., 2013). Several potential issues have been identified. These include the precipitation of sulfur upon direct vapor condensation, resulting in the deposition of elemental substances within and onto solid surfaces. Elevated blank concentrations may also occur due to the reagents used for sampling, particularly when volcanic gases are sampled into alkaline (NaOH) condensates, a common technique for sampling and analysis of major gases. Additionally, non-quantitative trapping of volatile elements into condensates can occur resulting in underestimation of the analyte content, while trapping of aerosol (rock particles from magma fragmentation or eroded from the conduit and/or condensed species from the magmatic gas) would overestimate the concentration of some elements with respect to pure gaseous compounds. Furthermore, analytical uncertainties and challenges often arise from the sample matrix, particularly with elevated concentrations of elements such as S, F and Na.

To assess data quality, we employed three different sampling approaches and compared the results (Table 1, Figs. 2 and 3). Firstly, direct condensation of volcanic gas was applied, followed by filtration (0.2 µm), dilution, and acidification with HNO_3. Secondly, samples were collected into pre-evacuated gas bottles containing a 25% NH_4OH solution, followed by dilution. Thirdly, samples were collected using condensation trap followed by traps containing an oxidizing agent (0.3M NaOCl) connected in-line. Subsequently, the samples were filtered and diluted. Direct condensate samples were obtained in 2008 and 2022, the samples being treated (filtered, diluted and acidified) on site after sampling in 2008 while they waited untreated for weeks after sampling in 2022. In 2009, only samples using condensation and NaOCl traps were collected, the condensate treated on site after sampling. In 2012, duplicate samples were collected, employing both pre-evacuated bottles containing NH_4OH and the previously described condensation traps and NaOCl traps, samples treated on site after sampling. Filtration directly after collection ensured removal of aerosol > 0.2 µm from the samples in 2008, 2009 and 2012.

Leaching of rock particles collected along with the condensate in 2022 would however have time to occur until filtration.

For alkali (Li, Na, K, Rb, Cs) and alkaline earth (Be, Mg, Ca, Sr, Ba) metals, the concentrations generally exhibit comparability among sampling methods. However, there are exceptions. Direct condensate samples, if not treated immediately like those from 2022, sometimes display concentration spikes for rock-forming elements (e.g. Li, Rb, Cs, Be, Mg, Sr, Mn, Fe, Al) which is likely related to host rock particle dissolution upon sample storage. This should be kept in mind when discussing gaseous transport solely. Additionally, samples collected into pre-evacuated gas bottles containing NH_4OH sometimes exhibit lower elemental concentrations, particularly for Ca and Mg. This decrease may be attributed to the precipitation of hydroxides in the alkaline condensate. For transition metals (Sc, Ti, V, Cr, Mn, Fe, Co, Ni, Cu, Zn, Zr, Nb, Mo, Ru, Rh, Pd, Ag, Cd, Hf, Ta, W, Re, Ir, Pt, Au and Hg), the concentrations are generally comparable among sampling methods. However, exceptions include concentration spikes (V, Cr, Fe, Nb, Hf) or lower concentrations (Co, Mo) in condensate samples. Nevertheless, concentration variability between samples, even during the same sampling campaign, is more noticeable than the variation between sampling methods. For post-transition metals (Al, Ga, Tl, Sn, Pb, Bi), metalloids (B, Si, Ge, As, Sb, Te), and non-metals (P, Se), the elemental concentrations often exhibit variability among methods. Some elements (Al, Ga, Sb) display concentration spikes in direct condensation samples, while others show low concentrations in NH_4OH (B, Al, Sn, P, Te) and NaOCl (Bi) samples. Regarding Rare Earth Elements and actinides (Y, La, Ce, Pr, Nd, Sm, Eu, Gd, Tb, Dy, Ho, Er, Tm, Yb, Lu, Th, U), they generally exhibit low and similar concentrations among different sampling methods. However, in some cases, concentrations are lower for samples collected into NH_4OH solution (Y, Ce, Ho, U).

Direct comparison of data for the same fumarole emission is possible for samples collected using condensation and NaOCl traps and pre-evacuated gas bottles containing NH_4OH (Fig. 3). The results reveal systematically higher concentrations for some elements in samples collected using the traps (Al, As, B, Ca, Cs, Ga, P, Pt, Rb, Sb, Si, Sn, Sr, Y, Yb, Zn), whereas other elements consistently display lower concentrations (Au, Bi, Mn, Hg, Pb, Tl). Selenium is often found at higher levels in NaOCl traps, while Hg and Pb tend to be more concentrated in NH_4OH bottles. Potassium and Ag show large variabilities between the two sampling methods. The use of an oxidizing agent (NaOCl) appears to be more effective to sample volatile elements such as As, Sb, and Se, which may partly remain in the gas phase at room temperature explaining the lower concentrations in NH_4OH bottles. However, the collection of mercury (Hg) is not efficient, suggesting the need for different methods for specific Hg studies (i.e., Edwards et al., 2023).

Our results emphasize the variability of trace element abundances measured in fumarolic gases. The efficiency in trapping elements is dependent on the sampling technique used. The analysis itself is not trivial, with some elements close to detection limits or with high uncertainties. Moreover, natural variations in fumarolic gas composition within short time scales can also lead to varying abundances. Trace element data for fumarolic gases should therefore be treated mindfully, our results suggesting a meaningful and reasonable range of one order of magnitude to be expected for most elements.

5.2. Trace element speciation in volcanic gas

The transport behavior of trace elements in volcanic gases is primarily influenced by the complexation of these elements with various ligands (Symonds et al., 1987, Wahrenberger et al., 2002, Henley and Seward, 2018, Mandon et al., 2020, Mason et al., 2021). Among the major ligands present in the volcanic gas at Vulcano are water, sulfur, chlorine, fluorine, and carbon. The concentrations of major species, and consequently the concentration of ligands, remain relatively constant during decompression and cooling as the gas ascends from depth to the surface (Fig. 4). Water (H_2O) stands out as the dominant gaseous species. Regarding chlorine, fluorine, and carbon, HCl, HF, and CO_2 predominate across the entire temperature and pressure range, with other Cl, F, and C species being of minor importance. As for sulfur, SO_2 dominates at higher temperatures, while H_2S becomes more significant as the temperature decreases, eventually leading to an SO_2/H_2S mole ratio of ~1 at temperatures below 350°C. The volcanic gas exhibits a reduced state, with measurable concentrations of H_2 (Table 1). However, precise modeling of the H_2 concentration, and indeed the relative abundance of redox-sensitive species (CO_2, CO, CH_4, SO_2, H_2S, H_2), depends greatly on the initial H_2 composition of the magmatic gas. In this context, we have established a value of 3000 µmol/mol to replicate H_2 concentrations (10^{-3} - 10^{-2} µmol/mol) and SO_2/H_2S ratios (0.7-35) at the sampling temperatures (~200-400°C) (Fig. 4). This magma value aligns with the measured H_2 content of arc magmas (Giggenbach and Guern, 1976, Taran et al., 1995, Fischer et al., 1998a, Henley and Hughes, 2016).

In contrast to major elements, the speciation of trace elements varies and depends on temperature (Fig. 5). Alkali metals are primarily transported as simple metal-chloride gaseous species, such as $LiCl_{(g)}$, $KCl_{(g)}$, $NaCl_{(g)}$, $RbCl_{(g)}$, and $CsCl_{(g)}$, from magmatic to surface temperatures. Fluorine becomes increasingly significant at lower temperatures, forming simple $KF_{(g)}$ species or more complex $LiAlF_{4(g)}$ compounds (Fig. 5, Table 2). On the other hand, alkaline earth metals are transported as chloride, hydrated, or mixed hydroxo-chloro compounds, including $Be(OH)_{2(g)}$, $Mg(OH)_{2(g)}$, $MgCl_{2(g)}$, $CaCl_{2(g)}$, $SrCl_{2(g)}$, and $CaCl(OH)_{(g)}$.

Most transition metals exist as hydroxide and/or chloride gaseous species at high temperatures, with chloride species becoming predominant as temperature decreases (Fig. 5). Additionally, sulfur and elemental species are present, and mixed hydroxo-chloro species are predicted to occur. These mixed species include $TiOCl_{2(g)}$, $VOCl_{(g)}$, $VOCl_{2(g)}$, $VOCl_{3(g)}$, and $NbOCl_{3(g)}$, while the transition from hydroxide to chloride species includes $Cr(OH)_{3(g)}$ to $CrCl_{3(g)}$, $Fe(OH)_{2(g)}$ to $FeCl_{2(g)}$, $Co(OH)_{2(g)}$ to $CoCl_{2(g)}$, $Ni(OH)_{2(g)}$ to $NiCl_{2(g)}$, $Cd(OH)_{2(g)}$ to $CdCl_{2(g)}$, and $Re(OH)_{3(g)}$ to $ReCl_{3(g)}$. Other transition metals are observed as single species from magmatic to surface temperatures, complexed with chloride, fluoride, hydroxide, and sulfide, or exist as elemental gas. These include $MnCl_{2(g)}$, $CuCl_{(g)}$, $ZnCl_{2(g)}$, $AgCl_{(g)}$, $WO_2(OH)_{2(g)}$, $AuS_{(g)}$, and $Hg_{(g)}$.

Post-transition metals, metalloids, and non-metals exhibit significantly more variability in gaseous speciation distribution compared to alkali, alkaline earth, and transition metals. Only a few are transported solely as hydrated or oxide gaseous species, such as $Al(OH)_{3(g)}$, $Si(OH)_{4(g)}$, $B(OH)_{3(g)}$, and $TlO_{(g)}$, along with chloride species like $GaCl_{3(g)}$ and $SbCl_{(g)}$. The remaining trace element groups show varying species occurrence depending on temperature. These include $PbS_{(g)}$ and $PbCl_{2(g)}$, $BiS_{(g)}$, $Bi_{(g)}$, and $BiCl_{3(g)}$, $AsS_{(g)}$, $AsO_{(g)}$, and $As_2S_{3(g)}$, $TeS_{(g)}$ and $TeCl_{2(g)}$, as well as $SeH_{(g)}$ and $SeS_{(g)}$. However, concerning the gaseous speciation of rare earth elements and actinides, limited data are available, and these are not included in the thermodynamic database used for the present work.

Our findings regarding the speciation of trace elements in volcanic gas align with previous studies (e.g., Symonds et al., 1987, Symonds et al., 1992, Wahrenberger et al., 2002,

Henley and Seward, 2018). However, the outcomes of both current and past research are contingent upon the thermodynamic database employed, the thermodynamic formulation applied, and the inclusion of gaseous species (Williams-Jones and Heinrich, 2005, Pokrovski et al., 2013). Thermodynamic data for trace elements are often insufficiently defined and missing for many elements and compounds in low-density water vapor characteristic of volcanic gases (ρ_w < 300 kg/m^3 at a few kilometers depth, ρ_w ~ 1 kg/m^3 at the surface)(e.g., Kestin et al., 1984, Palmer et al., 2004). Furthermore, water vapor at elevated temperatures is not simply hydrogen-bonded dielectric solvent, nor is it merely a gas. Instead, it comprises aggregates of water molecules held together by hydrogen bonding, forming water clusters. The size of these clusters increases with pressure at a given temperature as density increases, eventually exhibiting properties similar to liquid water. Conversely, decreasing pressure reduces the number of water molecules in the cluster until they approach unity, causing water vapor to approach the behavior of a gas (e.g., Lemke and Seward, 2018). The measured solubility of compounds in water vapor is notably higher than that predicted from the vapor pressure of the same compound over its respective crystalline solid melt. For instance, the sublimation solubility of $NaCl_{(s)}$ is x_{NaCl} = $5 \cdot 10^{-8}$ at 500°C and 1 bar, rising to $x_{NaCl} = 10^{-4}$ at 300 bar. This phenomenon suggests hydration of NaCl to form hydrated $NaCl \cdot (H_2O)_n$ compounds, with the number of water molecules in the compound increasing with pressure (Pitzer and Pabalan, 1986, Lemke and Seward, 2018, Velizhanin et al., 2020). Similar trends have been observed for other elements in water vapor, such as Fe, Zn, Cu (Pokrovski et al., 2005, Velizhanin et al., 2020), La, Nd, and Er (Alcorn et al., 2022). Consequently, the dominant gas species of trace elements may not be represented by a single gas compound (e.g. CuCl), as commonly assumed, including in this study. Instead, they may exist as a series of hydrated metal-ligand compounds (e.g. $CuCl \cdot nH_2O$). Extrapolating thermodynamic properties from liquid-like to vapor-like water, or from a low gaseous state to water vapor, may not be applicable for such fluids. It follows that the fundamental assumptions of the approaches used in the present study and previous work may be invalid, encompassing both the thermodynamic equations and the thermodynamic values (i.e., the thermodynamic database). These calculations heavily rely on extrapolating thermodynamic properties of gaseous compounds at low pressures to higher pressures, where hydration significantly impacts gas-species thermodynamic stabilities. However, the general lack of experimental data currently hinders the generation of such a thermodynamic database despite their importance for understanding, for example, element transport in volcanic water-rich vapor.

5.3. Gas-solid interaction

Thermodynamic calculations were further employed to gain insight into the gas-solid interaction and the condensation or formation of secondary mineral phases upon cooling and decompression of the magmatic gas.

Most trace elements were found to reach equilibrium with solid phases between 100-1000°C. At high temperatures, the reactions typically involve the formation of oxides, aluminum silicates, and sulfides (Figs. 6-8, Table 3). Quartz, Ca-Na-K feldspars, and Mg-pyroxene are predicted to be the most abundant at temperatures of ~700-1000°C, forming via reactions such as:

$$Si(OH)_{4(g)} = SiO_{2(s)} + 2H_2O_{(g)}$$

$$NaCl_{(g)} + Al(OH)_{3(g)} + 3Si(OH)_{4(g)} = NaAlSi_3O_{8(s)} + HCl_{(g)} + 7H_2O_{(g)}$$

$$KCl_{(g)} + Al(OH)_{3(g)} + 3Si(OH)_{4(g)} = KAlSi_3O_{8(s)} + HCl_{(g)} + 7H_2O_{(g)}$$
$$CaCl_{2(g)} + 2Al(OH)_{3(g)} + 2Si(OH)_{4(g)} = CaAl_2Si_2O_{8(s)} + 2HCl_{(g)} + 6H_2O_{(g)}$$
$$Mg(OH)_{2(g)} + Si(OH)_{4(g)} = MgSiO_{3(s)} + 3H_2O_{(g)}$$

The feldspars and pyroxene may potentially contain traces of other alkali and alkaline earth metals (Rb, Cs, Sr, and Ba) according to the thermodynamic calculations. Further decrease in temperature to below ~600-700°C results in abundant magnetite formation, along with other less abundant metal (V, Cr, Ga, W, and Sn) oxides:

$$3FeCl_{2(g)} + 4H_2O_{(g)} = Fe_3O_{4(s)} + 6HCl_{(g)} + H_{2(g)}$$

Decreasing temperature also leads to sulfide mineral formation, with the most abundant being Fe, Cu, and Cu-Fe containing sulfides (pyrite, chalcocite, and chalcopyrite):

$$FeCl_{2(g)} + 2H_2S_{(g)} = FeS_{2(s)} + 2HCl_{(g)} + H_{2(g)}$$
$$2CuCl_{(g)} + 2H_2S_{(g)} = Cu_2S_{(s)} + 2HCl_{(g)}$$
$$CuCl_{(g)} + FeCl_{2(g)} + 2H_2S_{(g)} = CuFeS_{2(s)} + 3HCl_{(g)} + \tfrac{1}{2}H_{2(g)}$$

Traces of other metal sulfides (Zn, Pb, Ni, Co, Cd, Mo, Ag, As, and Bi) are also present.

As the volcanic gas approaches the surface and further cools, decompression and gas expansion occur, along with sulfur oxidation and disproportionation. This results in characteristic argillic alteration with sulfates and sulfosalts becoming the most abundant secondary minerals from the volcanic gas, including alkali (Li, K, Na, Rb, and Cs), alkaline earth metals (Be, Mg, Ca, Sr, and Ba), transition metals (Mn, Fe, Zn,), and post-transition metals (Sn, Pb, and Bi) containing sulfates.

A variety of minerals have been identified at Vulcano in association with high-temperature fumarole emissions (100-600°C) (Garavelli and Vurro, 1994, Garavelli et al., 1997, Vurro et al., 1999, Cheynet et al., 2000, Garavelli et al., 2005, Pinto et al., 2014). These minerals include elemental sulfur (S), salammoniac (NH_4Cl), sassolite (H_3BO_3), various sulfides, and sulfosalts particularly enriched in certain metals (Pb, Bi, Zn, and Fe), oxychlorides. Examples of these minerals are bismuthinite (Bi_2S_3), cannizzarite ($Pb_{48}Bi_{56}S_{132}$), galenobismutite ($PbBi_2S_4$), lillianite ($Pb_3Bi_2S_6$), cosalite ($Pb_2Bi_2S_5$), galena (PbS), sphalerite (ZnS), wurtzite ((Zn,Fe)S), pyrite (FeS_2), anglesite ($PbSO_4$), baliczunicite ($Bi_2O(SO_4)_2$), bismoclite (BiOCl), among others. Small amounts of Se and Cd also occur in the sulfides. Our gas-solid modeling suggests the formation of such sulfides at temperatures below ~400-500°C and sulfosalts at temperatures below ~200-300°C, including galena, anglesite, bismuthinite, pyrite, sphalerite, and bismuth sulfate. However, the thermodynamic modeling fails to reproduce the detailed compositional variations of the observed sulfides, as well as the observed formation temperatures. For example, the modeling indicates galena as the predominant Pb-containing mineral over a relatively large temperature range of ~250-500°C, whereas galena is observed in natural sublimates collected in silica tubes inserted in fumaroles at narrow temperature range of ~400-500°C (Garavelli et al., 1997).This small discrepancy may be explained by different major gas composition between our study and that of Garavelli et al. (1997). Additionally, our modeling does not always replicate the observed mineral paragenesis, especially for rare minerals or those with complex formula. Similar controversies between gas-solid modeling and observations have been reported previously (Symonds and Reed, 1993, Wahrenberger et al., 2002). These are considered to result

from the limited number of minerals included in the thermodynamic database (e.g. no Pb-Bi sulfide species) used for the calculations, excluding most solid solutions, as well as the potentially inaccurate thermodynamic properties of many gaseous species. These differences in modeled versus observed mineralogy clearly indicate the need for improved thermodynamics of gas species in geologically relevant vapor phases.

The thermodynamic modeling and resulting mineral paragenesis are resembling what is observed in porphyry ore-forming environments. At high temperatures, feldspar alteration is predicted, similar to that observed along with abundant quartz, following significant sulfide mineralization at lower temperatures. These sulfides are enriched in Cu and Fe, along with other metals such as Pb, Zn, Cd, Co, Ni, Ag, Bi, and As. The volcanic fluids are acidic, which may be reflected in a more Na-Ca type alteration potentially lacking ore minerals, rather than the typical potassic alteration associated with high ore grades. Furthermore, the lower-temperature argillic alteration predicted as a consequence of cooling and oxidation is also typically observed at later stages and shallower depths relative to the sulfide mineralization (e.g., Seedorff et al., 2005).

Comparison of observed concentrations and those predicted by thermodynamic modeling further reveals important discrepancies. Trace element concentrations often display similar concentration despite large range in sampling temperature (100-550°C) whereas the thermodynamic modeling suggests rapid decrease in concentration resulting from mineralization upon cooling and decompression (Figs. 6-8). This trend suggests that trace element abundance in volcanic gases may not reflect gas-solid equilibria at sampling temperatures, but instead, the initial volcanic gas composition and/or gas-solid equilibria at higher temperatures than those reflecting the sampling conditions. For instance, the Si concentrations measured in fumarole emissions is typically ~$2 \cdot 10^4$ nmol/mol ($6 \cdot 10^2$ to $1.8 \cdot 10^5$ nmol/mol), resembling experimentally measured quartz solubility in water vapor at >800°C and >10 bar (Fig. 9), or higher equilibrium temperatures and pressures than those measured in fumarole emissions – more like the expected conditions within the gases at depth. Contribution from solid particles <0.2 μm transported alongside the gas phase cannot be ruled out, as our samples were not filtered for smaller particles. However, it is unlikely that all particles formed during the gas rise from source to surface are <0.2 μm in size and that none of them are deposited along the way. This suggests that the volcanic gas may indeed be in gas-solid equilibrium, at least for some major minerals, and that rapid expansion of the gas under close-to-surface conditions result in gas cooling, reflected in variable sampling temperatures, without quantitative mineral precipitation from the volcanic gas phase.

5.4. Trace element fluxes

Individual trace element fluxes were estimated based on their concentration to SO_2 ratio and SO_2 flux measurements. Sulfur dioxide emissions have been continuously monitored at Vulcano (Vita et al., 2012, Inguaggiato et al., 2022), with a value of 12±1 t/day during 2008-2012 and a sharp increase during the 2021-2022 unrest, with 79 t/day in 2022 (Aiuppa et al., 2022, Inguaggiato et al., 2022).

The four-year average survey of 2008-2012 reveals fluxes >100 kg/d for B and Al, between 10 and 100 kg/d for Fe and Si, between 1 and 10 kg/d for Zn, K, Bi, Ti, As, Ca, Mg, and Pb, between 0.1 and 1 kg/d for Sb, Li, Ni, Rb, Tl, Ta, Cr, Cu, Sr, Mn, Ba, and Na, and <0.1 kg/d for all other elements (Table 4, Fig. 10). Trace element emission rates are up to two orders of magnitude higher during the 2022 unrest compared to 2008-2012, except for B, As, Zn, Sb, Tl,

Se, Sn and Mo which exhibit similar fluxes. Notably, Vulcano emitted > 10 kg/d of Pb and Bi in February 2022. Most rock-forming elements display elevated emission rates during the 2022 unrest, but these are uncertain and subject to contamination related to mineral dissolution upon sample storage.

Emission rates obtained in this study fall within the range of those measured previously in 1993 (Cheynet et al., 2000) for As, Bi, Cd, Pb, Tl, and Zn, indicating consistency over the past 30 years of activity. However, these fluxes are minor compared to nearby Stromboli and Etna, where SO_2 emission rates of 300 and 1000-4560 t/d, respectively, have been recorded (Buat-Ménard and Arnold, 1978, Bergametti et al., 1984, Andres et al., 1993, Gauthier and Le Cloarec, 1998, Allard et al., 2000, Calabrese et al., 2011, Calabrese et al., 2015) and subsequently much greater trace element fluxes (Fig. 10). Trace element emission rates at these volcanoes exceed those of Vulcano by over 100 times and sometimes over 1000 times for elements such as Li, K, Na, Rb, Cs, Mg, Ca, Sr, Ba, V, Cr, Mn, Fe, Co, Ni, Cu, Zn, Mo, Ag, Cd, W, Re, Au, Hg, Tl, Sn, and Se. In contrast, fluxes of Pb, Bi, B, As, Sb, and Te are not as dwarfed by those of Stromboli and Etna, with at most an order and a half of magnitude difference. Therefore, despite its relatively low SO_2 fluxes, Vulcano should be considered a high-emission volcano for these elements.

6. Conclusions

The geochemistry of trace elements in volcanic gas at Vulcano (Sicily, Italy) was investigated through the analysis of fumarole emissions (94 to 412°C), coupled with thermodynamic modeling. Trace element concentrations vary across ten orders of magnitude, ranging from ~0.01 pmol/mol to ~300 µmol/mol, with certain metalloids being the most abundant. They are followed by alkali and alkaline earth metals, along with specific transition metals, while rare earth elements and actinides typically exhibit the lowest concentrations.

Determining trace element concentrations in volcanic gas emissions depends on the sampling and sample storage methods employed. Condensates are susceptible to post-sampling alterations unless treated immediately. Sampling into alkaline condensate (NH_4OH) may lead to precipitation and the loss of certain elements during sample storage. Conversely, trapping using oxidizing agents (NaOCl) results in effective sampling of volatile elements, albeit with analytical challenges due to the complex sample matrix.

Thermodynamic modeling suggests that most trace elements are transported as chloride, hydroxide, and mixed hydroxy-chloro gas species, with sulfides, hydrates, and elemental gas species also playing significant roles for some elements. However, the gaseous speciation of many trace elements remains uncertain or unknown due to a lack of thermodynamic data.

Upon cooling and decompression of the volcanic gas, most trace elements are expected to reach gas-solid equilibrium, leading to the formation of secondary minerals. At high temperatures (~700-1000°C), the dominant mineral assemblage comprises quartz, Ca-Na-K feldspars, and Mg-pyroxene, with minor concentrations of other alkali and alkaline earth metals. Subsequent cooling and decompression result in the formation of magnetite, pyrite, chalcocite, and chalcopyrite, alongside other less abundant oxides. Eventually, a range of sulfates and sulfosalts is formed at the lowest temperatures (~100-300°C). For most trace elements, fumarole emission concentrations reflect higher gas-solid equilibrium temperatures than those observed during sampling, indicating gas-solid equilibria at high temperatures followed by incomplete re-

equilibration upon further cooling near the surface. By mass, only a small portion of the trace elements are condensing to form minerals, the majority staying in the gas phase until emission at the fumarole outlet.

Trace element fluxes span over seven orders of magnitude, ranging from approximately 1·10-6 kg/day to >100 kg/day, and are consistent with previous reports. Silica, Al, and B consistently exhibit the highest fluxes, followed by alkali and alkaline earth metals, various transition metals and metalloids, with rare earth elements and actinides displaying the lowest fluxes. Overall, the trace element fluxes are lower compared to neighboring Stromboli and Etna, except for Pb, Bi, B, As, Sb, and Te.

Acknowledgements

The authors would like to thank all the people involved during the sampling campaigns, especially Walter d'Alessandro. Special thanks to Fabio Vita for the SO_2 fluxes for the dates of interest. Celine Mandon would like to express her gratitude and appreciation for Terry Seward for introducing her into the world of volcanic gas transport, and for his kindness and support as a supervisor and mentor. This study was supported by The Icelandic Centre for Research (#0902290) and Nordic Volcanic Center. The authors would like to thank Tobias Fischer for editorial handling, Michael Zelenski and an anonymous reviewer for their thoughtful reviews which greatly improve the quality of the manuscript.

References

Africano, F., Van Rompaey, G., Bernard, A.,Le Guern, F., (2002). Deposition of trace elements from high temperature gases of Satsuma-Iwojima volcano. *Earth, Planets and Space 54*(3), 275-286.

Aiuppa, A., (1999). Trace element geochemistry of volcanic fluids released by eastern Sicilian volcanoes (southern Italy). PhD Thesis, Univ. Palermo.

Aiuppa, A., Bitetto, M., Calabrese, S., Delle Donne, D., Lages, J., La Monica, F. P., Chiodini, G., Tamburello, G., Cotterill, A., Fulignati, P., Gioncada, A., Liu, E. J., Moretti, R.,Pistolesi, M., (2022). Mafic magma feeds degassing unrest at Vulcano Island, Italy. *Communications Earth & Environment 3*(1), 255.

Aiuppa, A., Dongarrà, G., Capasso, G.,Allard, P., (2000). Trace elements in the thermal groundwaters of Vulcano Island (Sicily). *Journal of Volcanology and Geothermal Research 98*(1), 189-207.

Aiuppa, A., Federico, C., Giudice, G.,Gurrieri, S., (2005). Chemical mapping of a fumarolic field: La Fossa Crater, Vulcano Island (Aeolian Islands, Italy). *Geophysical Research Letters 32*(13).

Alcorn, C. D., Velizhanin, K. A., Strzelecki, A. C., Nisbet, H. D., Currier, R. P., Roback, R. C.,Migdisov, A. A., (2022). An experimental study of the solubility of rare earth chloride salts (La, Nd, Er) in HCl bearing water vapor from 350 to 425 °C. *Geochimica et Cosmochimica Acta 330*, 6-26.

Allard, P., Aiuppa, A., Loyer, H., Carrot, F., Gaudry, A., Pinte, G., Michel, A.,Dongarrà, G., (2000). Acid gas and metal emission rates during long-lived basalt degassing at Stromboli Volcano. *Geophysical Research Letters 27*(8), 1207-1210.

Allen, A. G., Baxter, P. J.,Ottley, C. J., (2000). Gas and particle emissions from Soufrière Hills Volcano, Montserrat, West Indies: characterization and health hazard assessment. *Bulletin of Volcanology 62*(1), 8-19.

Andres, R. J., Kyle, P. R.,Chuan, R. L., (1993). Sulphur dioxide, particle and elemental emissions from Mount Etna, Italy during July 1987. *Geologische Rundschau 82*(4), 687-695.

Arnórsson, S., Bjarnason, J. Ö., Giroud, N., Gunnarsson, I.,Stefánsson, A., (2006). Sampling and analysis of geothermal fluids. *Geofluids 6*(3), 203-216.

Badalamenti, B., Chiodini, G., Cioni, R., Favara, R., Francofonte, S., Gurrieri, S., Hauser, S., Inguaggiato, S., Italiano, F.,Magro, G., (1991). Special field workshop at Vulcano (Aeolian Islands) during summer 1988: geochemical results. *Acta Vulcanologica 1*, 223-227.

Barberi, F., Neri, G., Valenza, M.,Villari, L., (1991). 1987–1990 unrest at Vulcano. Acta Vulcanol. *Acta vulcanologica 1*, 95-106.

Bergametti, G., Martin, D., Carbonnelle, J., Faivre-Pierret, R.,Le Sage, R. V., (1984). A mesoscale study of the elemental composition of aerosols emitted from Mt. Etna Volcano. *Bulletin Volcanologique 47*(4), 1107-1114.

Blundy, J.,Wood, B., (2003). Partitioning of trace elements between crystals and melts. *Earth and Planetary Science Letters 210*(3), 383-397.

Bobrowski, N., Honninger, G., Galle, B.,Platt, U., (2003). Detection of bromine monoxide in a volcanic plume. *Nature 423*(6937), 273-276.

Brondi, M.,Dall'Aglio, M., (1991). Evolution of mercury, arsenic, antimony, radon and helium contents in ground waters and fumaroles since 1983 through 1989 at Vulcano Island (Southern Italy). *Acta Vulcanol. 1*, 233-241.

Buat-Ménard, P.,Arnold, M., (1978). The heavy metal chemistry of atmospheric particulate matter emitted by Mount Etna Volcano. *Geophysical Research Letters 5*(4), 245-248.

Calabrese, S., Aiuppa, A., Allard, P., Bagnato, E., Bellomo, S., Brusca, L., D'Alessandro, W.,Parello, F., (2011). Atmospheric sources and sinks of volcanogenic elements in a basaltic volcano (Etna, Italy). *Geochimica et Cosmochimica Acta 75*(23), 7401-7425.

Calabrese, S., Scaglione, S., Milazzo, S., Alessandro, W., Bobrowski, N., Giuffrida, G. B., Tedesco, D., Parello, F.,Yalire, M., (2015). Passive degassing at Nyiragongo (D.R. Congo) and Etna (Italy) volcanoes. *2015 57*.

Capasso, G., Dongarrà, G., Favara, R., Hauser, S.,Valenza, M., (1992). Isotope composition of rain water, well water and fumarole steam on the island of Vulcano, and their implications for volcanic surveillance. *Journal of Volcanology and Geothermal Research 49*(1), 147-155.

Capasso, G., Favara, R., Francofonte, S.,Inguaggiato, S., (1999). Chemical and isotopic variations in fumarolic discharge and thermal waters at Vulcano Island (Aeolian Islands, Italy) during 1996: evidence of resumed volcanic activity. *Journal of Volcanology and Geothermal Research 88*(3), 167-175.

Capasso, G., Favara, R.,Inguaggiato, S., (1997). Chemical features and isotopic composition of gaseous manifestations on Vulcano Island, Aeolian Islands, Italy: An interpretative model of fluid circulation. *Geochimica et Cosmochimica Acta 61*(16), 3425-3440.

Carapezza, M., Nuccio, P. M.,Valenza, M., (1981). Genesis and evolution of the fumaroles of vulcano (Aeolian Islands, Italy): a geochemical model. *Bulletin Volcanologique 44*(3), 547-563.

Cheynet, B., Dall'Aglio, M., Garavelli, A., Grasso, M. F.,Vurro, F., (2000). Trace elements from fumaroles at Vulcano Island (Italy): rates of transport and a thermochemical model. *Journal of Volcanology and Geothermal Research 95*(1-4), 273-283.

Chiodini, G., Cioni, R., Falsaperla, S., Montalto, A., Guidi, M.,Marini, L., (1992). Geochemical and seismological investigations at Vulcano (Aeolian Islands) during 1978–1989. *Journal of Geophysical Research: Solid Earth 97*(B7), 11025-11032.

Chiodini, G., Cioni, R.,Marini, L., (1993). Reactions governing the chemistry of crater fumaroles from Vulcano Island, Italy, and implications for volcanic surveillance. *Applied Geochemistry 8*(4), 357-371.

Chiodini, G., Cioni, R., Marini, L.,Panichi, C., (1995). Origin of the fumarolic fluids of Vulcano Island, Italy and implications for volcanic surveillance. *Bulletin of Volcanology 57*(2), 99-110.

Cioni, R.,D'Amore, F., (1984). A genetic model for the crater fumaroles of Vulcano island (Sicily, Italy). *Geothermics 13*(4), 375-384.

Clocchiatti, R., Del Moro, A., Gioncada, A., Joron, J. L., Mosbah, M., Pinarelli, L.,Sbrana, A., (1994). Assessment of a shallow magmatic system: the 1888–90 eruption, Vulcano Island, Italy. *Bulletin of Volcanology 56*(6), 466-486.

Costa, S., Masotta, M., Gioncada, A., Pistolesi, M., Bosch, D.,Scarlato, P., (2020). Magma evolution at La Fossa volcano (Vulcano Island, Italy) in the last 1000 years: evidence from eruptive products and temperature gradient experiments. *Contributions to Mineralogy and Petrology 175*(4), 31.

De Astis, G., Lucchi, F., Dellino, P., La Volpe, L., Tranne, C. A., Frezzotti, M. L.,Peccerillo, A., (2013). Geology, volcanic history and petrology of Vulcano (central Aeolian archipelago). *Geological Society, London, Memoirs 37*(1), 281-349.

Delmelle, P., Stix, J.,Gases, J. V., (2000). Encyclopedia of volcanoes, Academic Press: San Diego.

Demartin, F., Gramaccioli, C. M.,Campostrini, I., (2009). Brontesite,(NH4) 3PbCl5, a new product of fumarolic activity from La Fossa crater, Vulcano, Aeolian Islands, Italy. *The Canadian Mineralogist 47*(5), 1237-1243.

Dongarrà, G.,Varrica, D., (1998). The presence of heavy metals in air particulate at Vulcano island (Italy). *Science of The Total Environment 212*(1), 1-9.

Edwards, B. A., Pfeffer, M. A., Jóhannsson, þ., Outridge, P. M.,Wang, F., (2023). An inter-method comparison of mercury measurements in Icelandic volcanic gases. *Applied Geochemistry 152*, 105654.

Falcone, E. E., Federico, C.,Boudoire, G., (2022). Geochemistry of trace metals and Rare Earth Elements in shallow marine water affected by hydrothermal fluids at Vulcano (Aeolian Islands, Italy). *Chemical Geology 593*, 120756.

Federico, C., Capasso, G., Paonita, A.,Favara, R., (2010). Effects of steam-heating processes on a stratified volcanic aquifer: Stable isotopes and dissolved gases in thermal waters of Vulcano Island (Aeolian archipelago). *Journal of Volcanology and Geothermal Research 192*(3), 178-190.

Federico, C., Cocina, O., Gambino, S., Paonita, A., Branca, S., Coltelli, M., Italiano, F., Bruno, V., Caltabiano, T., Camarda, M., Capasso, G., De Gregorio, S., Diliberto, I. S., Di Martino, R. M. R., Falsaperla, S., Greco, F., Pecoraino, G., Salerno, G., Sciotto, M., Bellomo, S., Grazia, G. D., Ferrari, F., Gattuso, A., La Pica, L., Mattia, M., Pisciotta, A. F., Pruiti, L.,Sortino, F., (2023). Inferences on the 2021 Ongoing Volcanic Unrest at Vulcano Island (Italy) through a Comprehensive Multidisciplinary Surveillance Network. *Remote Sensing 15*(5), 1405.

Fischer, T. P., Giggenbach, W. F., Sano, Y.,Williams, S. N., (1998a). Fluxes and sources of volatiles discharged from Kudryavy, a subduction zone volcano, Kurile Islands. *Earth and Planetary Science Letters 160*(1), 81-96.

Fischer, T. P., Shuttleworth, S.,O'Day, P. A., (1998b). Determination of trace and platinum-group elements in high ionic-strength volcanic fluids by sector-field inductively coupled plasma mass spectrometry (ICP-MS). *Fresenius' Journal of Analytical Chemistry 362*(5), 457-464.

Fulignati, P.,Sbrana, A., (1998). Presence of native gold and tellurium in the active high-sulfidation hydrothermal system of the La Fossa volcano (Vulcano, Italy). *Journal of Volcanology and Geothermal Research 86*(1), 187-198.

Fulignati, P., Sbrana, A., Clocchiatti, R.,Luperini, W., (2006). Environmental impact of the acid fumarolic plume of a passively degassing volcano (Vulcano Island, Italy). *Environmental Geology 49*(8), 1139-1155.

Garavelli, A., Laviano, R.,Vurro, F., (1997). Sublimate deposition from hydrothermal fluids at the Fossa Crater, Vulcano, Italy. *European Journal of Mineralogy 9*(2), 423-432.

Garavelli, A., Mozgova, N. N., Orlandi, P., Bonaccorsi, E., Pinto, D., MoëLo, Y.,Borodaev, Y. S., (2005). Rare sulfosalts from Vulcano, Aeolian Islands, Italy. VI. Vurroite, Pb20Sn2(Bi,As)22S54Cl6, A new mineral species. *The Canadian Mineralogist 43*(2), 703-711.

Garavelli, A.,Vurro, F., (1994). Barberiite, NH4BF4, a new mineral from Vulcano, Aeolian Islands, Italy. *American Mineralogist 79*(3-4), 381-384.

Gauthier, P.-J.,Le Cloarec, M.-F., (1998). Variability of alkali and heavy metal fluxes released by Mt. Etna volcano, Sicily, between 1991 and 1995. *Journal of Volcanology and Geothermal Research 81*(3-4), 311-326.

Gauthier, P.-J., Sigmarsson, O., Gouhier, M., Haddadi, B.,Moune, S., (2016). Elevated gas flux and trace metal degassing from the 2014–2015 fissure eruption at the Bárðarbunga volcanic system, Iceland. *Journal of Geophysical Research: Solid Earth 121*(3), 1610-1630.

Gemmell, J. B., (1987). Geochemistry of metallic trace elements in fumarolic condensates from Nicaraguan and Costa Rican volcanoes. *Journal of Volcanology and Geothermal Research 33*(1-3), 161-181.

Getahun, A., Reed, M. H.,Symonds, R., (1996). Mount St. Augustine volcano fumarole wall rock alteration: mineralogy, zoning, composition and numerical models of its formation process. *Journal of Volcanology and Geothermal Research 71*(2-4), 73-107.

Giggenbach, W. F.,Guern, F. L., (1976). The chemistry of magmatic gases from Erta'Ale, Ethiopia. *Geochimica et Cosmochimica Acta 40*(1), 25-30.

Granieri, D., Carapezza, M. L., Chiodini, G., Avino, R., Caliro, S., Ranaldi, M., Ricci, T.,Tarchini, L., (2006). Correlated increase in CO2 fumarolic content and diffuse emission from La Fossa crater (Vulcano, Italy): Evidence of volcanic unrest or increasing gas release from a stationary deep magma body? *Geophysical Research Letters 33*(13).

Hedenquist, J. W., Aoki, M.,Shinohara, H., (1994). Flux of volatiles and ore-forming metals from the magmatic-hydrothermal system of Satsuma Iwojima volcano. *Geology 22*(7), 585-588.

Henley, R. W.,Fischer, T. P., (2021). Sulfur sequestration and redox equilibria in volcanic gases. *Journal of Volcanology and Geothermal Research 414*, 107181.

Henley, R. W.,Hughes, G. O., (2016). SO2 flux and the thermal power of volcanic eruptions. *Journal of Volcanology and Geothermal Research 324*, 190-199.

Henley, R. W.,Seward, T. M., (2018). *Gas–Solid Reactions in Arc Volcanoes: Ancient and Modern*. P. L. King, Fegley B.,Seward T. M. High Temperature Gas-Solid Reactions in Earth and Planetary Processes. Reviews in Mineralogy and Geochemistry: Mineralogical Society of America. 84**,** 309-349.

Hinkley, T. K., Lamothe, P. J., Wilson, S. A., Finnegan, D. L.,Gerlach, T. M., (1999). Metal emissions from Kilauea, and a suggested revision of the estimated worldwide metal output by quiescent degassing of volcanoes. *Earth and Planetary Science Letters 170*(3), 315-325.

Ilyinskaya, E., Mason, E., Wieser, P. E., Holland, L., Liu, E. J., Mather, T. A., Edmonds, M., Whitty, R. C. W., Elias, T., Nadeau, P. A., Schneider, D., McQuaid, J. B., Allen, S. E., Harvey, J., Oppenheimer, C., Kern, C.,Damby, D., (2021). Rapid metal pollutant deposition from the volcanic plume of Kīlauea, Hawai'i. *Communications Earth & Environment 2*(1), 78.

Inguaggiato, S., Vita, F., Diliberto, I. S., Mazot, A., Calderone, L., Mastrolia, A.,Corrao, M., (2022). The Extensive Parameters as a Tool to Monitoring the Volcanic Activity: The Case Study of Vulcano Island (Italy). *Remote Sensing 14*(5), 1283.

Inostroza, M., Aguilera, F., Menzies, A., Layana, S., González, C., Ureta, G., Sepúlveda, J., Scheller, S., Böehm, S., Barraza, M., Tagle, R.,Patzschke, M., (2020). Deposition of metals and metalloids in the fumarolic fields of Guallatiri and Lastarria volcanoes, northern Chile. *Journal of Volcanology and Geothermal Research 393*, 106803.

Italiano, F., Pecoraino, G.,Nuccio, P. M., (1998). Steam output from fumaroles of an active volcano: Tectonic and magmatic-hydrothermal controls on the degassing system at Vulcano (Aeolian arc). *Journal of Geophysical Research: Solid Earth 103*(B12), 29829-29842.

Iveson, A. A., Webster, J. D., Rowe, M. C.,Neill, O. K., (2019). Fluid-melt trace-element partitioning behaviour between evolved melts and aqueous fluids: Experimental constraints on the magmatic-hydrothermal transport of metals. *Chemical Geology 516*, 18-41.

Kaasalainen, H.,Stefánsson, A., (2012). The chemistry of trace elements in surface geothermal waters and steam, Iceland. *Chemical Geology 330-331*, 60-85.

Kestin, J., Sengers, J. V., Kamgar-Parsi, B.,Sengers, J. M. H. L., (1984). Thermophysical Properties of Fluid H2O. *Journal of Physical and Chemical Reference Data 13*(1), 175-183.

Lemke, K. H.,Seward, T. M., (2018). *Molecular Clusters and Solvation in Volcanic and Hydrothermal Vapors*. P. King, Fegley B.,Seward T. M. Reviews in Mineralogy and Geochemistry: Mineralogical Society of America. 84**,** 57-83.

Mandon, C. L., Christenson, B. W., Schipper, C. I., Seward, T. M.,Garaebiti, E., (2019). Metal transport in volcanic plumes: A case study at White Island and Yasur volcanoes. *Journal of Volcanology and Geothermal Research 369*, 155-171.

Mandon, C. L., Seward, T. M.,Christenson, B. W., (2020). Volatile transport of metals and the Cu budget of the active White Island magmatic-hydrothermal system, New Zealand. *Journal of Volcanology and Geothermal Research 398*, 106905.

Martini, M., Piccardi, G.,Legittimo, P. C., (1980). Geochemical surveillance of active volcanoes: data on the fumaroles of Vulcano (Aeolian Islands, Italy). *Bulletin Volcanologique 43*(1), 255-263.

Mason, E., Wieser, P. E., Liu, E. J., Edmonds, M., Ilyinskaya, E., Whitty, R. C. W., Mather, T. A., Elias, T., Nadeau, P. A., Wilkes, T. C., McGonigle, A. J. S., Pering, T. D., Mims, F. M., Kern, C., Schneider, D. J.,Oppenheimer, C., (2021). Volatile metal emissions from volcanic degassing and lava–seawater interactions at Kīlauea Volcano, Hawai'i. *Communications Earth & Environment 2*(1), 79.

Mather, T. A., Pyle, D. M.,Oppenheimer, C., (2003). Tropospheric Volcanic Aerosol. *Geophysical Monograph-American Geophysical Union 139*, 189-212.

Mather, T. A., Witt, M. L. I., Pyle, D. M., Quayle, B. M., Aiuppa, A., Bagnato, E., Martin, R. S., Sims, K. W. W., Edmonds, M., Sutton, A. J.,Ilyinskaya, E., (2012). Halogens and trace metal emissions from the ongoing 2008 summit eruption of Kīlauea volcano, Hawai`i. *Geochimica et Cosmochimica Acta 83*(0), 292-323.

Nash, W. P.,Crecraft, H. R., (1985). Partition coefficients for trace elements in silicic magmas. *Geochimica et Cosmochimica Acta 49*(11), 2309-2322.

Nriagu, J. O., (1989). A global assessment of natural sources of atmospheric trace metals. *Nature 338*(6210), 47-49.

Nuccio, P. M., Paonita, A.,Sortino, F., (1999). Geochemical modeling of mixing between magmatic and hydrothermal gases: the case of Vulcano Island, Italy. *Earth and Planetary Science Letters 167*(3), 321-333.

Palmer, D. A., Simonson, J. M.,Jensen, J. P., (2004). *Chapter 12 - Partitioning of electrolytes to steam and their solubilities in steam*. D. A. P. F.-P. H. Harvey. Aqueous Systems at Elevated Temperatures and Pressures. London: Academic Press**,** 409-439.

Paonita, A., Favara, R., Nuccio, P. M.,Sortino, F., (2002). Genesis of fumarolic emissions as inferred by isotope mass balances: CO2 and water at Vulcano Island, Italy. *Geochimica et Cosmochimica Acta 66*(5), 759-772.

Paonita, A., Federico, C., Bonfanti, P., Capasso, G., Inguaggiato, S., Italiano, F., Madonia, P., Pecoraino, G.,Sortino, F., (2013). The episodic and abrupt geochemical changes at La Fossa fumaroles (Vulcano Island, Italy) and related constraints on the dynamics, structure, and compositions of the magmatic system. *Geochimica et Cosmochimica Acta 120*, 158-178.

Peccerillo, A., Frezzotti, M. L., De Astis, G.,Ventura, G., (2006). Modeling the magma plumbing system of Vulcano (Aeolian Islands, Italy) by integrated fluid-inclusion geobarometry, petrology, and geophysics. *Geology 34*(1), 17-20.

Pinto, D., Garavelli, A.,Mitolo, D., (2014). Balićžunićite, Bi2O(SO4)2, a new fumarole mineral from La Fossa crater, Vulcano, Aeolian Islands, Italy. *Mineralogical Magazine 78*(4), 1043-1055.

Pitzer, K. S.,Pabalan, R. T., (1986). Thermodynamics of NaCl in steam. *Geochimica et Cosmochimica Acta 50*(7), 1445-1454.

Pokrovski, G. S., Borisova, A. Y.,Bychkov, A. Y., (2013). Speciation and Transport of Metals and Metalloids in Geological Vapors. *Reviews in Mineralogy and Geochemistry 76*(1), 165-218.

Pokrovski, G. S., Roux, J.,Harrichoury, J.-C., (2005). Fluid density control on vapor-liquid partitioning of metals in hydrothermal systems. *Geology 33*(8), 657-660.

Quisefit, J. P., Toutain, J. P., Bergametti, G., Javoy, M., Cheynet, B.,Person, A., (1989). Evolution versus cooling of gaseous volcanic emissions from Momotombo Volcano, Nicaragua: Thermochemical model and observations. *Geochimica et Cosmochimica Acta 53*(10), 2591-2608.

Rendel, P. M.,Mountain, B. W., (2023). Solubility of quartz in supercritical water from 375 °C to 600 °C and 200–270 bar. *The Journal of Supercritical Fluids 196*, 105883.

Seedorff, E., Dilles, J. H., Proffett, J. M., Einaudi, M. T., Zurcher, L., Stavast, W. J. A., Johnson, D. A.,Barton, M. D., (2005). Porphyry deposits: Characteristics and origin of hypogene features. *Economic Geology 100th anniversary volume*, 251-298.

Sortino, F., Nonell, A., Toutain, J. P., Munoz, M., Valladon, M.,Volpicelli, G., (2006). A new method for sampling fumarolic gases: Analysis of major, minor and metallic trace elements with ammonia solutions. *Journal of Volcanology and Geothermal Research 158*(3–4), 244-256.

Stoiber, R. E.,Rose, W. I., (1974). Fumarole incrustations at active central american volcanoes. *Geochimica et Cosmochimica Acta 38*(4), 495-516.

Symonds, R. B., Gerlach, T. M.,Reed, M. H., (2001). Magmatic gas scrubbing: implications for volcano monitoring. *Journal of Volcanology and Geothermal Research 108*(1-4), 303-341.

Symonds, R. B., Mizutani, Y.,Briggs, P. H., (1996). Long-term geochemical surveillance of fumaroles at Showa-Shinzan dome, Usu volcano, Japan. *Journal of Volcanology and Geothermal Research 73*(3), 177-211.

Symonds, R. B.,Reed, M. H., (1993). Calculation of multicomponent chemical equilibria in gas-solid-liquid systems; calculation methods, thermochemical data, and applications to studies of high-temperature volcanic gases with examples from Mount St. Helens. *American Journal of Science 293*(8), 758-864.

Symonds, R. B., Reed, M. H.,Rose, W. I., (1992). Origin, speciation, and fluxes of trace-element gases at Augustine volcano, Alaska: Insights into magma degassing and fumarolic processes. *Geochimica et Cosmochimica Acta 56*(2), 633-657.

Symonds, R. B., Rose, W. I., Bluth, G. J. S.,Gerlach, T. M., (1994). *Volcanic-gas studies: methods, results, and applications*. M. R. Carroll,Holloway J. R. Volatiles in magmas: Mineralogical Society of America. 30**,** 1-66.

Symonds, R. B., Rose, W. I., Reed, M. H., Lichte, F. E.,Finnegan, D. L., (1987). Volatilization, transport and sublimation of metallic and non-metallic elements in high temperature gases at Merapi Volcano, Indonesia. *Geochimica et Cosmochimica Acta 51*(8), 2083-2101.

Taran, Y. A., (2011). N2, Ar, and He as a tool for discriminating sources of volcanic fluids with application to Vulcano, Italy. *Bulletin of Volcanology 73*(4), 395-408.

Taran, Y. A., Hedenquist, J. W., Korzhinsky, M. A., Tkachenko, S. I.,Shmulovich, K. I., (1995). Geochemistry of magmatic gases from Kudryavy volcano, Iturup, Kuril Islands. *Geochimica et Cosmochimica Acta 59*(9), 1749-1761.

Varrica, D., Aiuppa, A.,Dongarrà, G., (2000). Volcanic and anthropogenic contribution to heavy metal content in lichens from Mt. Etna and Vulcano island (Sicily). *Environmental Pollution 108*(2), 153-162.

Velizhanin, K. A., Alcorn, C. D., Migdisov, A. A.,Currier, R. P., (2020). Rigorous analysis of non-ideal solubility of sodium and copper chlorides in water vapor using Pitzer-Pabalan model. *Fluid Phase Equilibria 522*, 112731.

Vita, F., Inguaggiato, S., Bobrowski, N., Calderone, L., Galle, B.,Parello, F., (2012). Continuous SO2 flux measurements for Vulcano Island, Italy. *Annals of Geophysics 55*(2), 301-308.

Vurro, F., Garavelli, A., Garbarino, C., Moelo, Y.,Borodaev, Y. S., (1999). Rare sulfosalts from Vulcano, Aeolian Islands, Italy. II. Mozgovaite, PbBi~ 4 (S, Se)~ 7, a new mineral species. *Canadian Mineralogist 37*(6), 1499-1506.

Wahrenberger, C., Seward, T. M.,Dietrich, V., (2002). *Volatile trace-element transport in high-temperature gases from Kudriavy volcano (Iturup, Kurile Islands, Russia)*. R. Hellmann,Wood S. A. Water–Rock Interaction: a Tribute to David A. Crerar: Geochemical Society Special Publication. 7**,** 307-327.

Wahrenberger, C. M., (1997). Some aspects of the chemistry of volcanic gases. PhD thesis, ETH Zurich.

Williams-Jones, A. E.,Heinrich, C. A., (2005). Vapor Transport of Metals and the Formation of Magmatic-Hydrothermal Ore Deposits. *Economic Geology 100*(7), 1287-1312.

Zanon, V., Frezzotti, M.-L.,Peccerillo, A., (2003). Magmatic feeding system and crustal magma accumulation beneath Vulcano Island (Italy): Evidence from CO2 fluid inclusions in quartz xenoliths. *Journal of Geophysical Research: Solid Earth 108*(B6).

Zelenski, M., Fischer, T. P., de Moor, J. M., Marty, B., Zimmermann, L., Ayalew, D., Nekrasov, A. N.,Karandashev, V. K., (2013). Trace elements in the gas emissions from the Erta Ale volcano, Afar, Ethiopia. *Chemical Geology 357*, 95-116.

Zelenski, M., Malik, N.,Taran, Y., (2014). Emissions of trace elements during the 2012–2013 effusive eruption of Tolbachik volcano, Kamchatka: enrichment factors, partition coefficients and aerosol contribution. *Journal of Volcanology and Geothermal Research 285*, 136-149.

Zelenski, M., Simakin, A., Taran, Y., Kamenetsky, V. S.,Malik, N., (2021). Partitioning of elements between high-temperature, low-density aqueous fluid and silicate melt as derived from volcanic gas geochemistry. *Geochimica et Cosmochimica Acta 295*, 112-134.

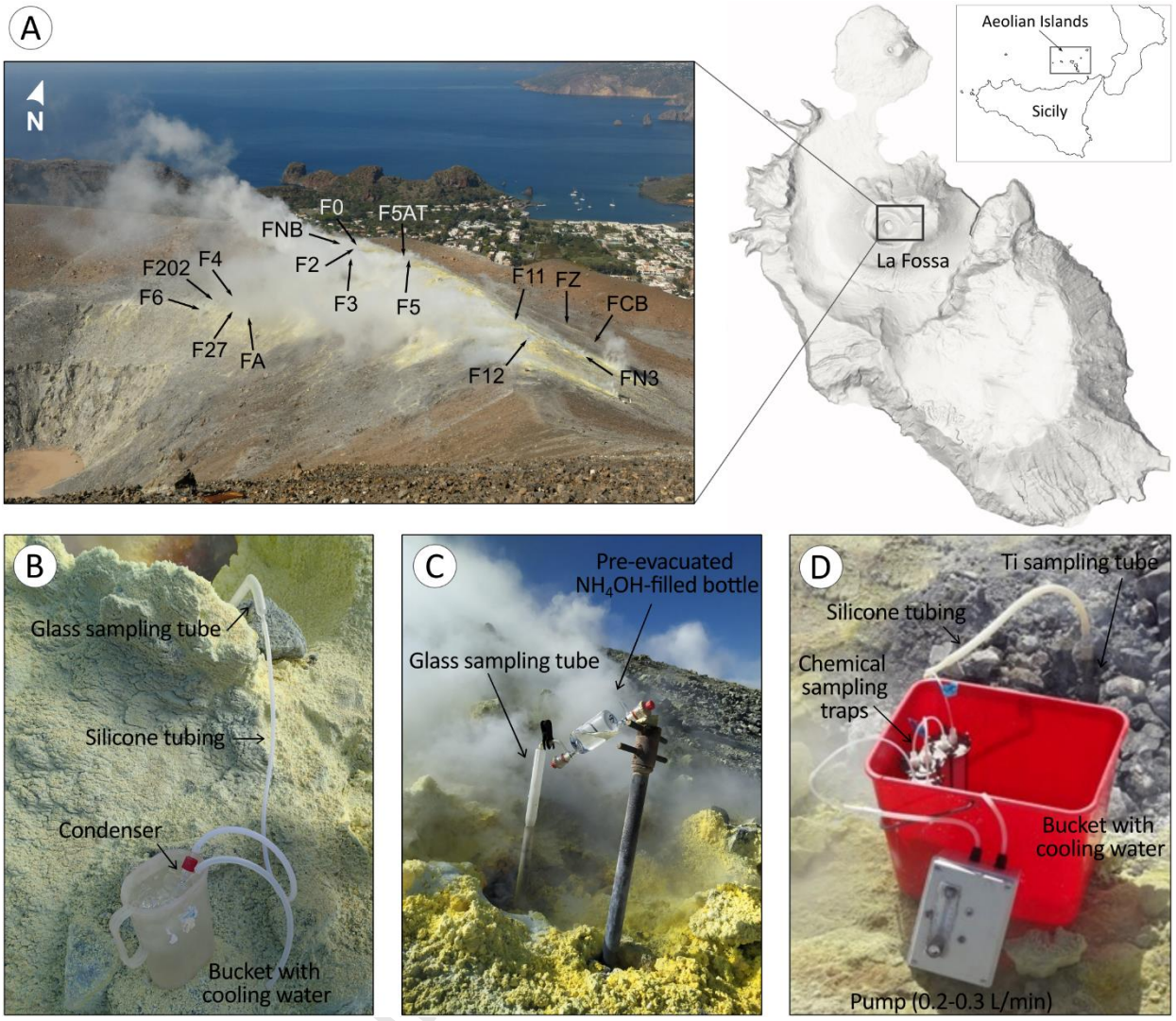

Fig. 1. Location of the study area of La Fossa, Vulcano (Sicily, Italy). A) Vulcano island and the location of fumaroles sampled at the La Fossa crater. B) Sampling setup for direct condensation, C) sampling setup for pre-evacuated gas bottles containing ~25% NH_4OH (30 ml per 100 ml bottle), D) sampling setup for in-line traps consisting of direct condensation followed by two traps containing 0.3M NaOCl with flow maintained at the end of the line using an air-pump.

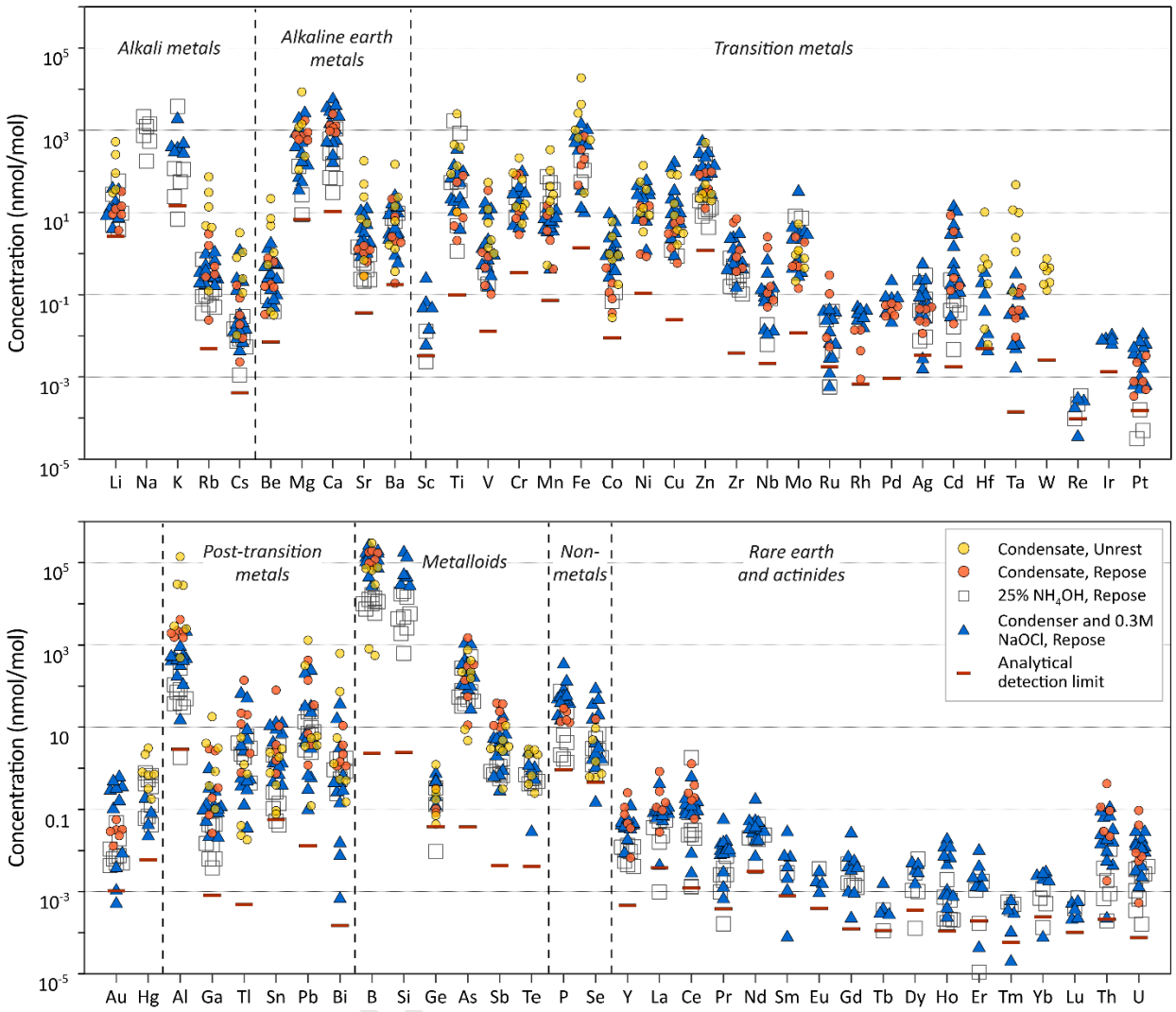

Fig. 2. Trace element concentrations of fumarolic emissions from Vulcano (Sicily, Italy). Shown are the results of variable sampling methods, whether samples were collected during a period of repose or unrest, and analytical detection limits.

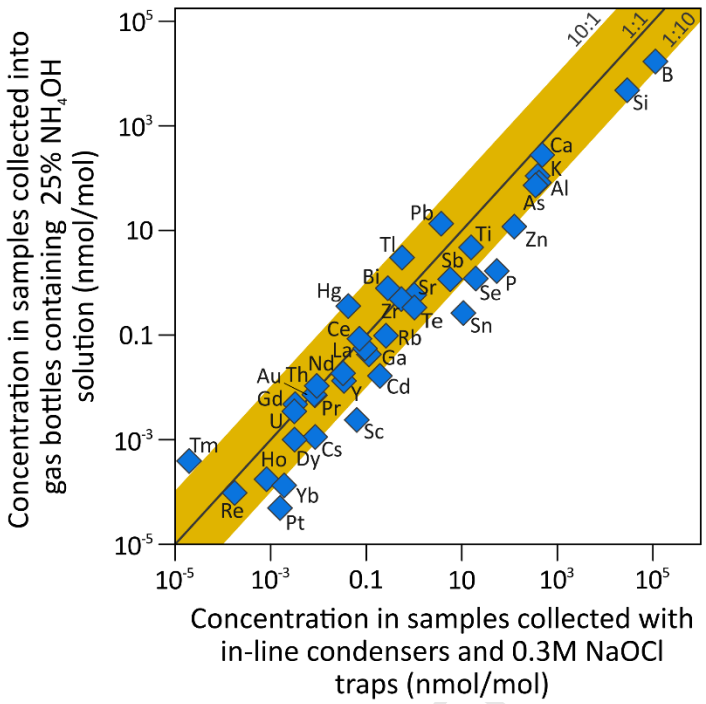

Fig. 3. Comparison between concentrations of trace elements from fumarole F2 (12-VUL-2) collected in pre-evacuated gas sampling bottles containing 25% NH_4OH (~30 ml in 100 ml bottle) and samples collected with a condenser and two traps containing 0.3M NaOCl.

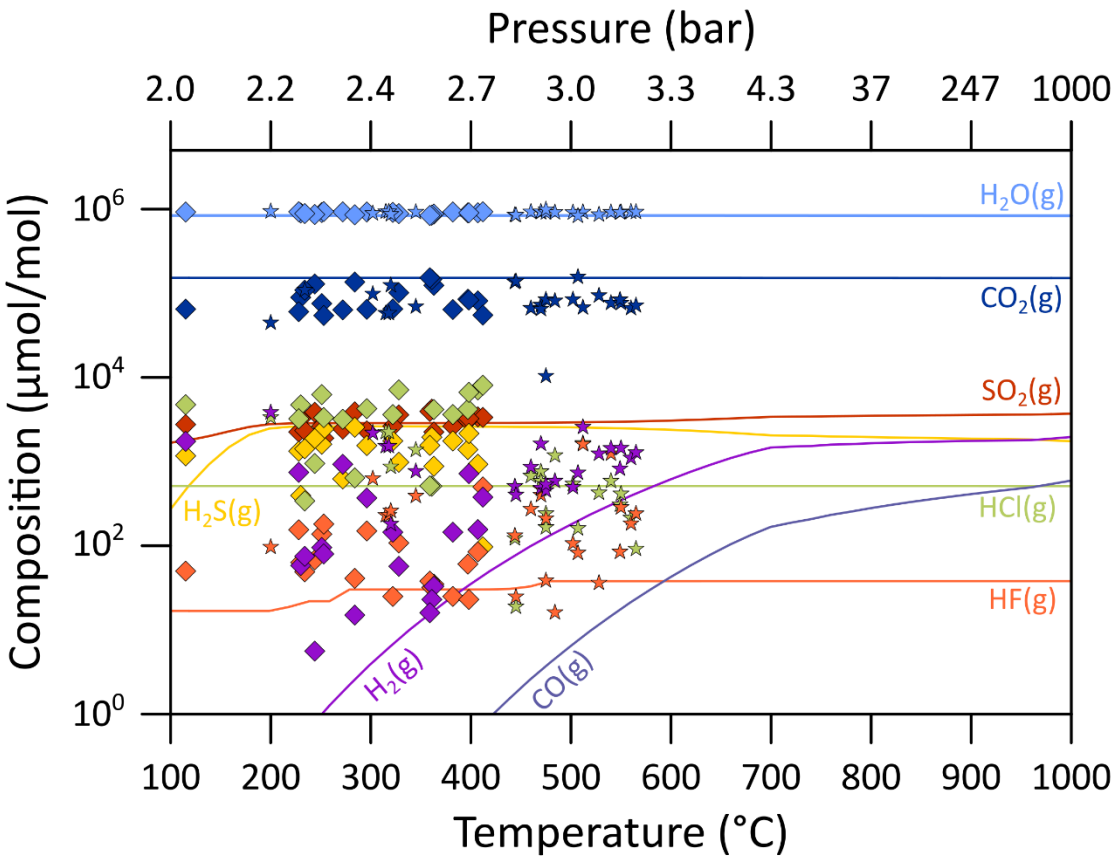

Fig. 4. The concentration of major gas species in volcanic gases at Vulcano (Sicily) as a function of temperature and decompression from magmatic temperatures (1000°C and 1 kbar) to surface (100-300°C and 2 bar). Note the non-linearity of the pressure scale, following the P-T path used for thermodynamic modelling and detailed in Supplementary material. The results of the thermodynamic calculations are shown as lines and the measured composition of fumarole discharges as symbols (diamond, this study, Table 1; star, data from Wahrenberger (1997)).

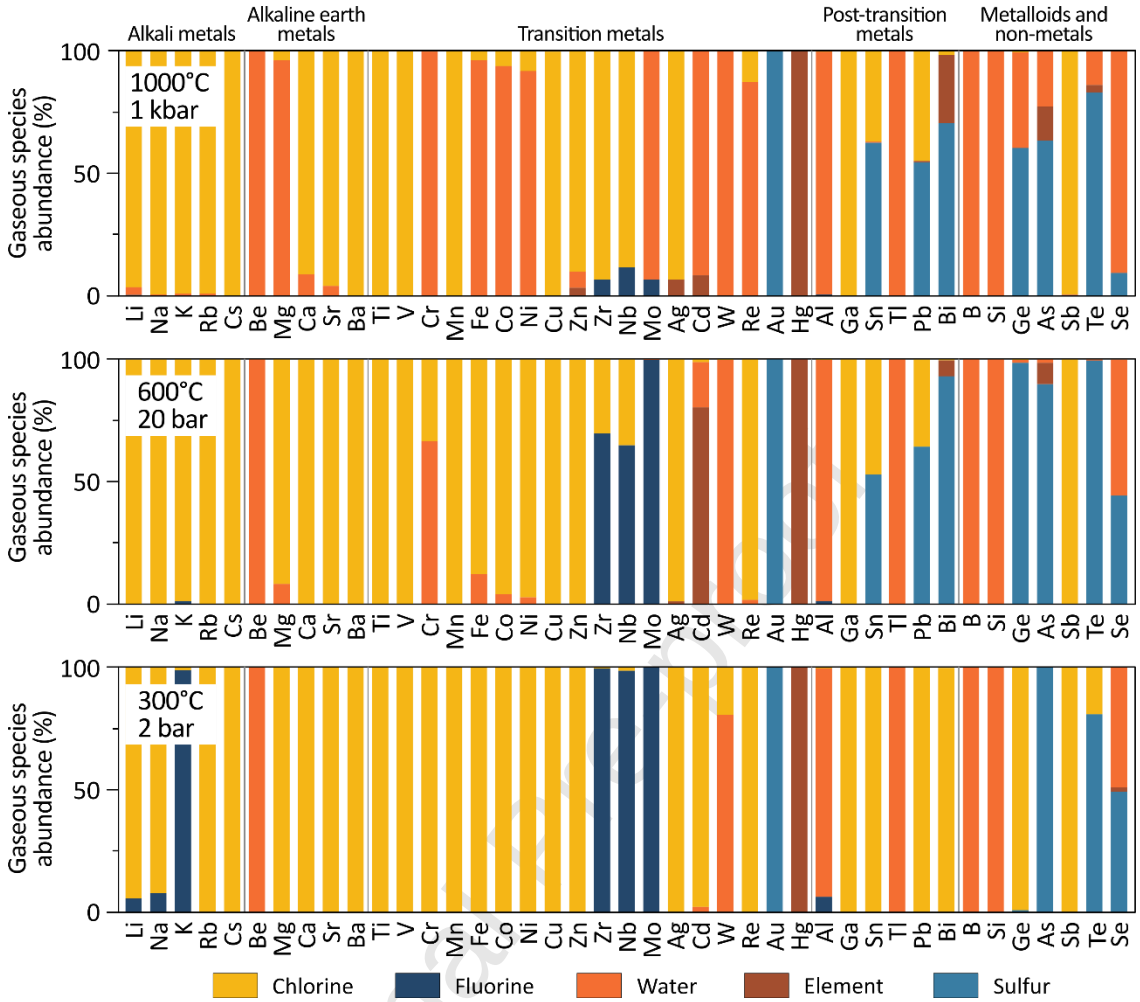

Fig. 5. The results of equilibrium gaseous species distribution of trace elements in volcanic gases at Vulcano (Sicily) at magmatic temperature and pressure (1000°C and 1 kbar), in the gas conduit (600°C and 20 bar) and at surface (300°C and 2 bar). The gaseous species have been grouped according to the predominant ligands of various species.

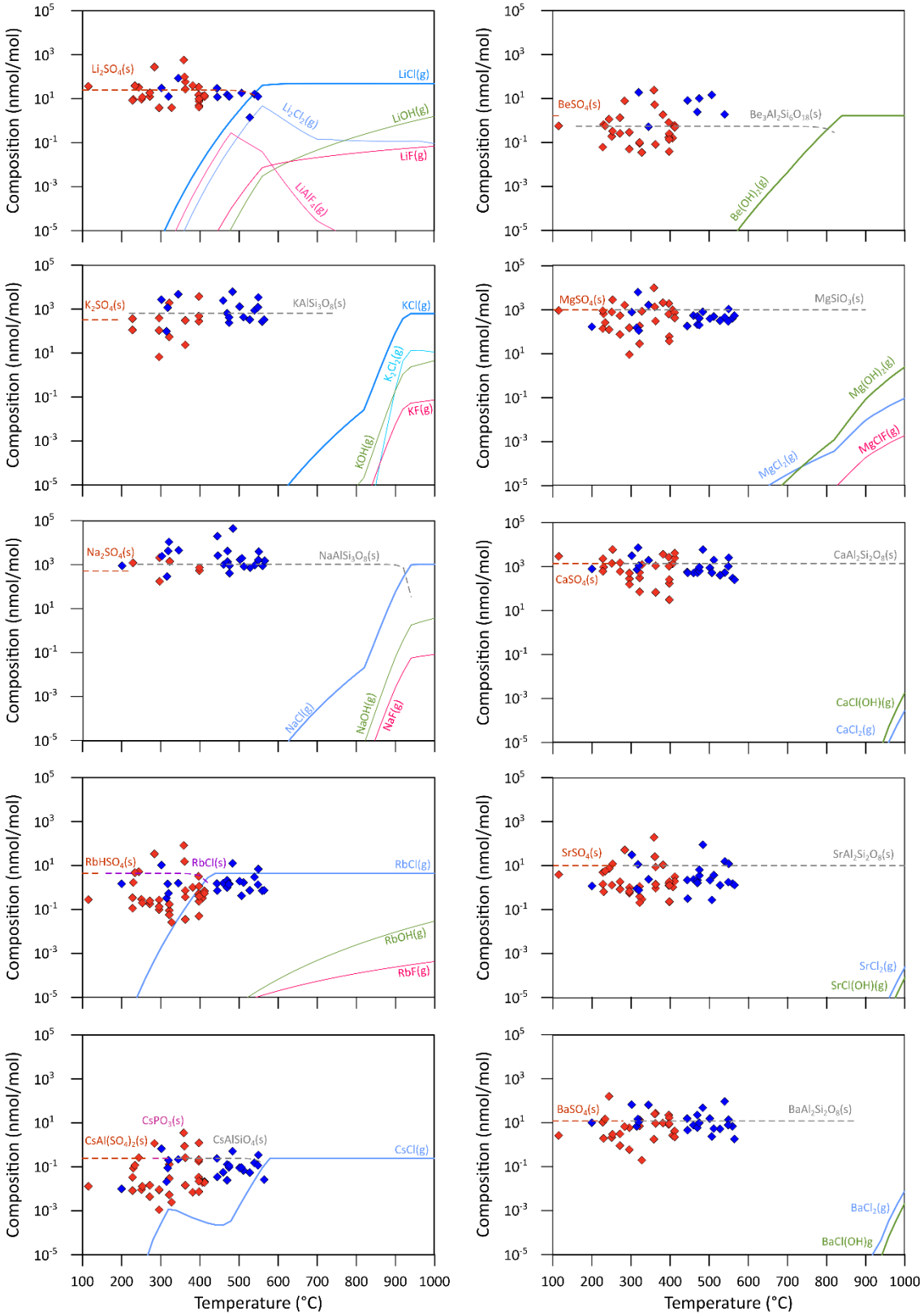

Fig. 6. The results of gas speciation and solid precipitation from thermodynamic modeling as a function of temperature and decompression from magmatic conditions (1000°C and 1 kbar) to

surface (100-300°C and 2 bar) for alkali (Li, Na, K, Rb, Cs) and alkaline earth (Be, Mg, Ca, Sr, Ba) metals. Curves show the concentrations of various gaseous species and solids and the diamonds the measured concentration in fumarole emissions (this study in red and Wahrenberger (1997) in blue).

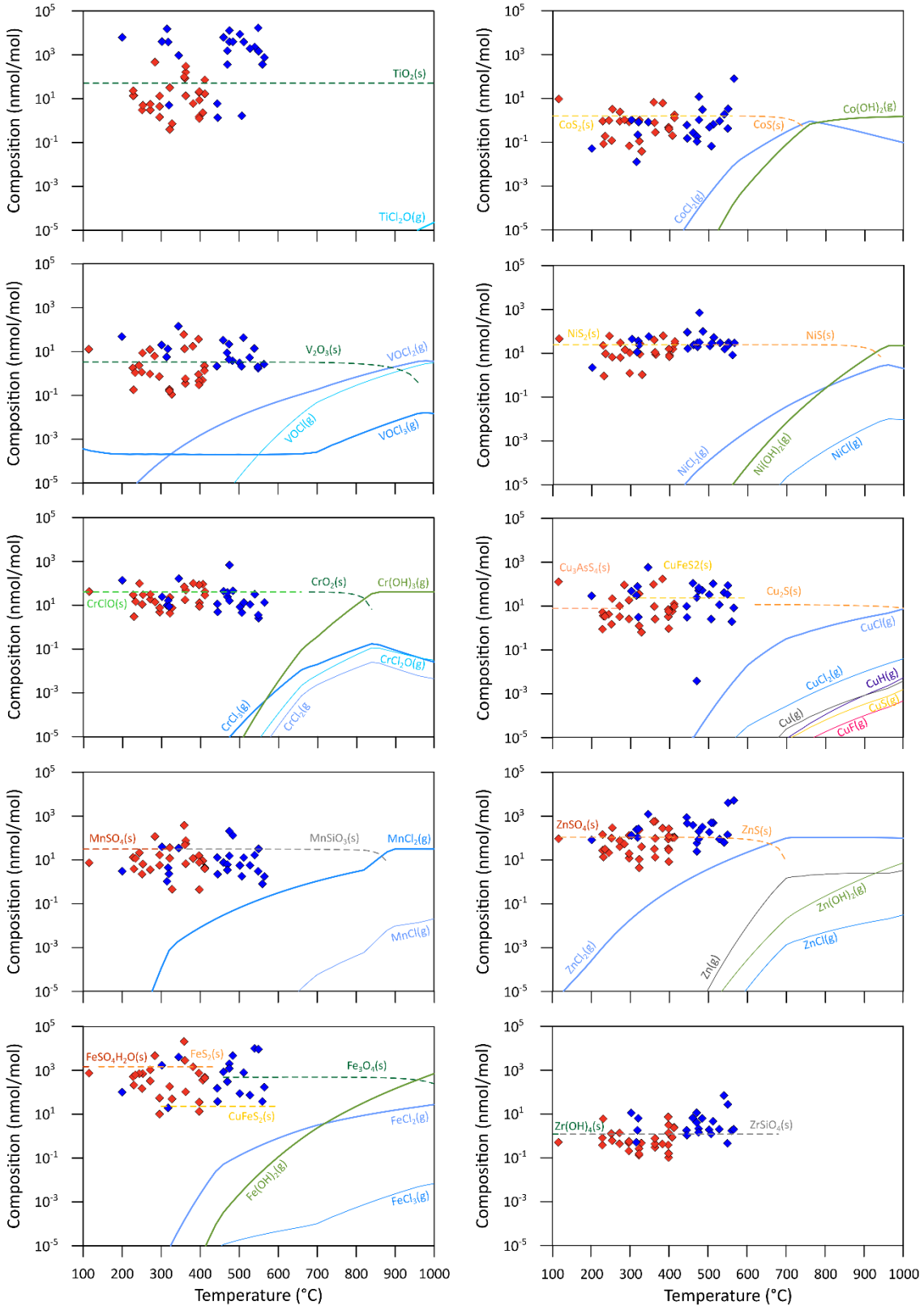
Composition (nmol/mol)
Temperature (°C)
TiO2(s)
TiCl2O(g)
CoS2(s)
CoS(s)
Co(OH)2(g)
CoCl2(g)
V2O3(s)
VOCl2(g)
VOCl(g)
VOCl3(g)
NiS2(s)
NiS(s)
NiCl2(g)
Ni(OH)2(g)
NiCl(g)
CrClO(s)
CrO2(s)
Cr(OH)3(g)
CrCl2O(g)
CrCl3(g)
CrCl2(g)
Cu3AsS4(s)
CuFeS2(s)
Cu2S(s)
CuCl(g)
CuCl2(g)
CuH(g)
Cu(g)
CuS(g)
CuF(g)
MnSO4(s)
MnSiO3(s)
MnCl2(g)
MnCl(g)
ZnSO4(s)
ZnS(s)
Zn(OH)2(g)
ZnCl2(g)
Zn(g)
ZnCl(g)
FeSO4H2O(s)
FeS2(s)
Fe3O4(s)
CuFeS2(s)
FeCl3(g)
Fe(OH)3(g)
FeCl3(g)
Zr(OH)4(s)
ZrSiO4(s)

Fig. 7

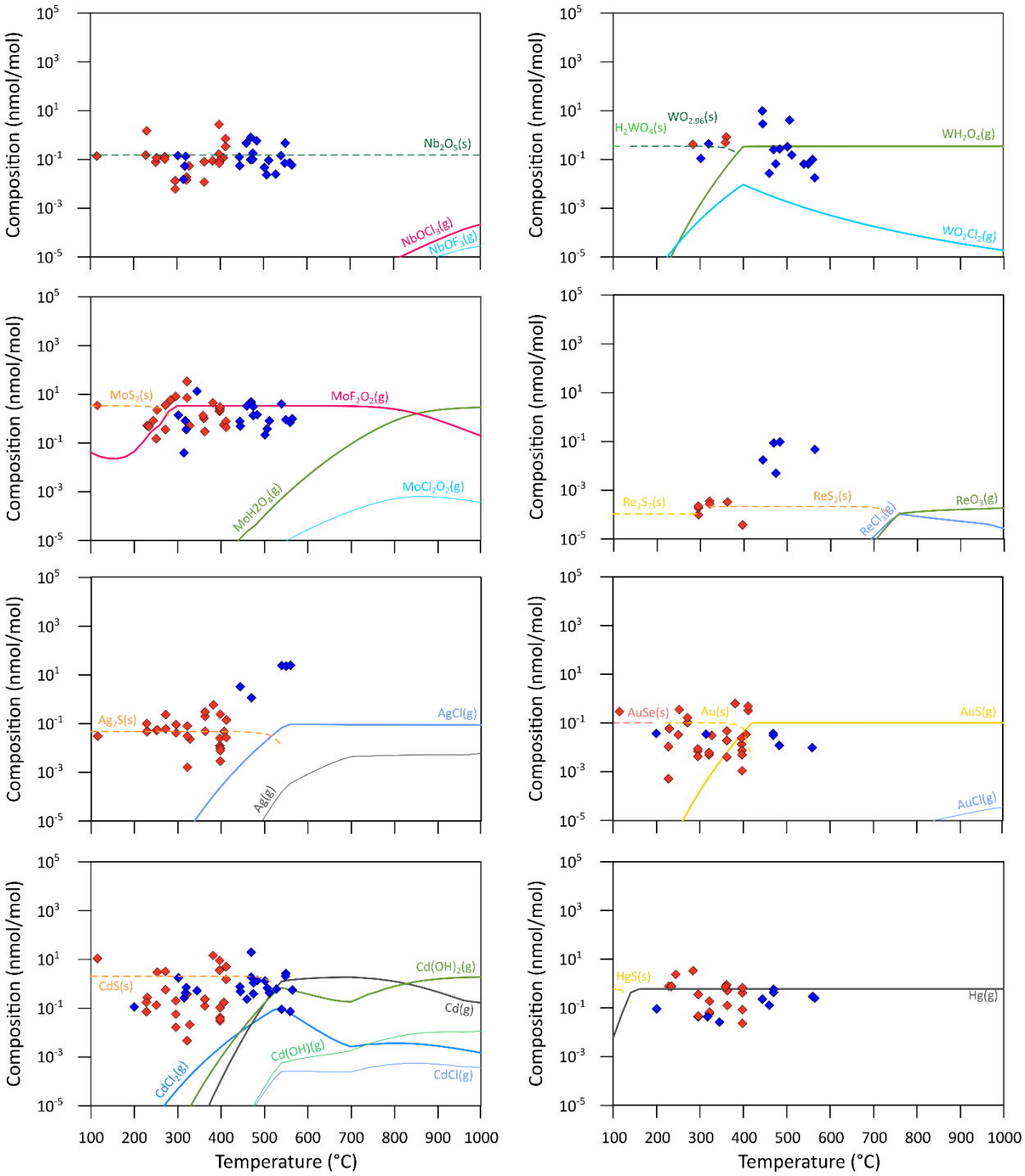

Fig. 7. The results of gas speciation and solid precipitation from thermodynamic modeling as a function of temperature and decompression from magmatic conditions (1000°C and 1 kbar) to surface (100-300°C and 2 bar) for transition metals (Ti, V, Cr, Mn, Fe, Co, Ni, Cu, Zn, Zr, Nb, Mo, Ag, Cd, W, Re, Au, Hg). Curves show the concentrations of various gaseous species and solids and the diamonds the measured concentration in fumarole emissions (this study in red and Wahrenberger (1997) in blue).

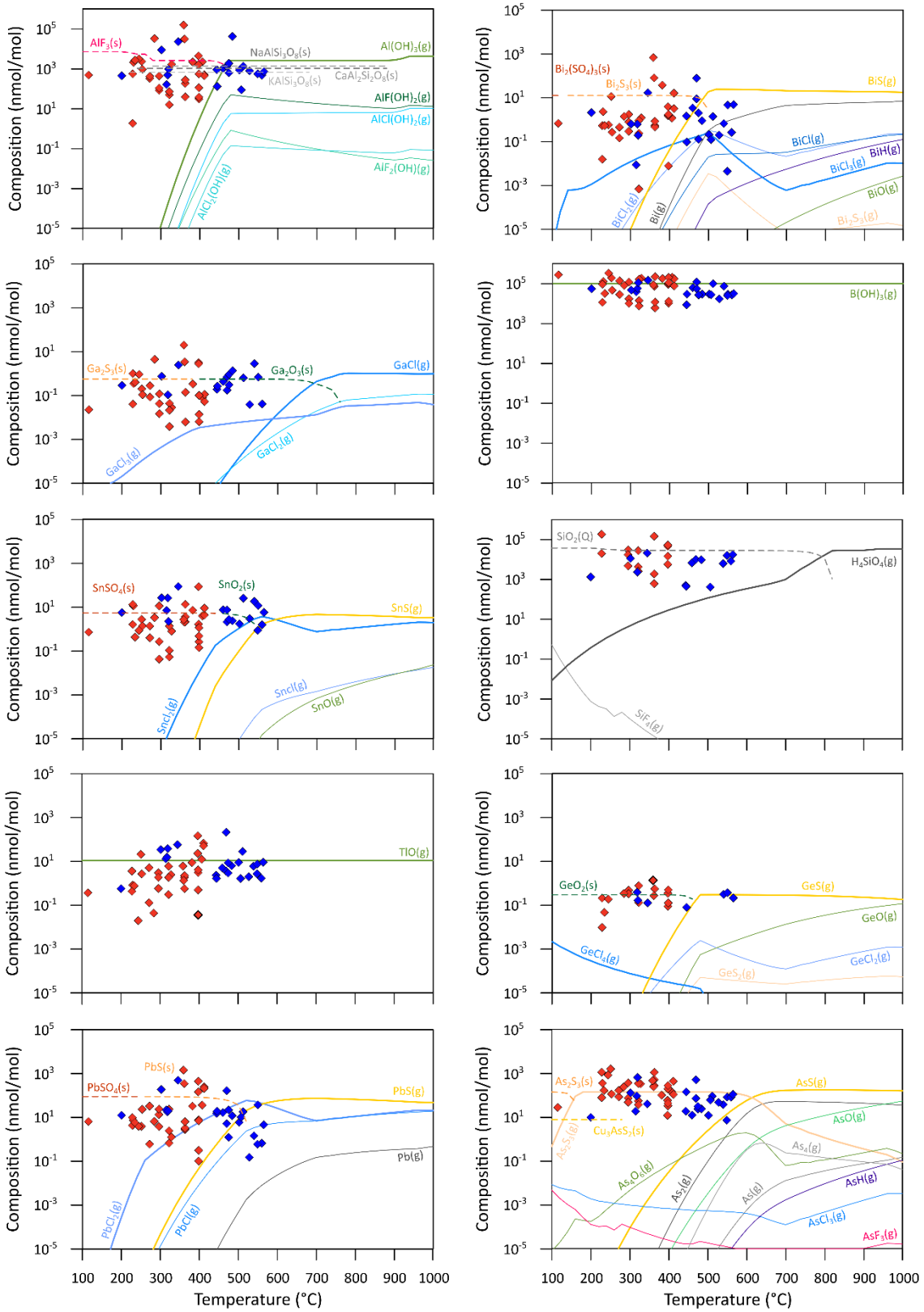
Composition (nmol/mol)
Temperature (°C)
AlF3(s)
NaAlSi3O8(s)
KAlSi3O8(s)
CaAl2Si2O8(s)
Al(OH)3(g)
AlF(OH)2(g)
AlCl(OH)2(g)
AlCl2(OH)(g)
AlF2(OH)(g)
Bi2(SO4)3(s)
Bi2S3(s)
BiS(g)
BiCl(g)
BiH(g)
BiCl3(g)
BiO(g)
BiCl2(g)
Bi(g)
Bi2S3(g)
Ga2S3(s)
Ga2O3(s)
GaCl(g)
GaCl3(g)
GaCl2(g)
B(OH)3(g)
SnSO4(s)
SnO2(s)
SnS(g)
SnCl2(g)
SnCl(g)
SnO(g)
SiO2(Q)
H4SiO4(g)
SiF4(g)
TlO(g)
GeO2(s)
GeS(g)
GeO(g)
GeCl4(g)
GeCl2(g)
GeS2(g)
PbS(s)
PbSO4(s)
PbS(g)
Pb(g)
PbCl2(g)
PbCl(g)
As2S3(s)
Cu3AsS3(s)
As2S3(g)
AsS(g)
AsO(g)
As4(g)
As4O6(g)
As2S2(g)
As(g)
AsH(g)
AsCl3(g)
AsF3(g)

Fig. 8

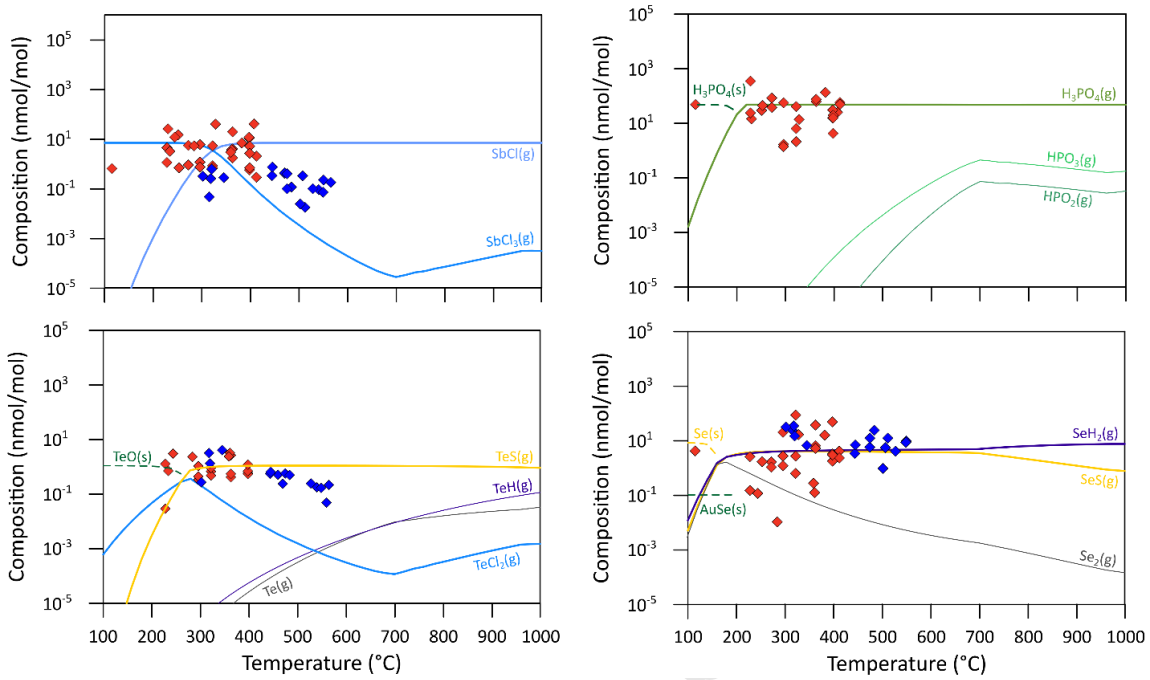

Fig. 8. The results of gas speciation and solid precipitation from thermodynamic modeling as a function of temperature and decompression from magmatic conditions (1000°C and 1 kbar) to surface (100-300°C and 2 bar) for post-transition metals, metalloids and non-metals. Curves show the concentrations of various gaseous species and solids and the diamonds the measured concentration in fumarole emissions (this study in red and Wahrenberger (1997) in blue).

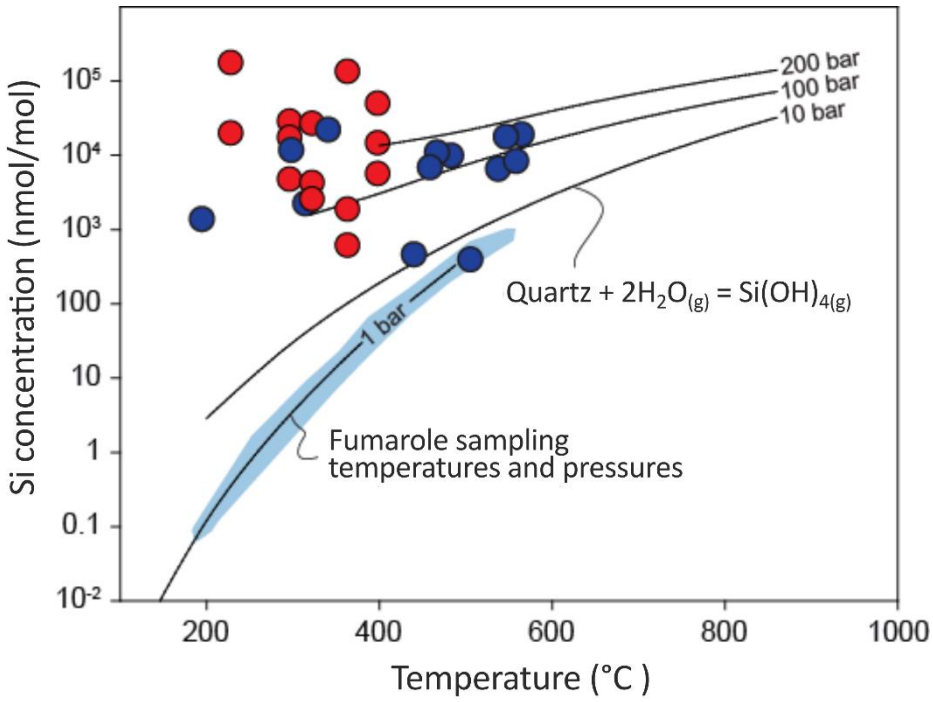

Fig. 9. The concentrations of silica in the volcanic gas fumarole emissions (dots) and in water vapor in equilibrium with quartz (curves) as a function of temperature and pressure (Rendel and Mountain, 2023).

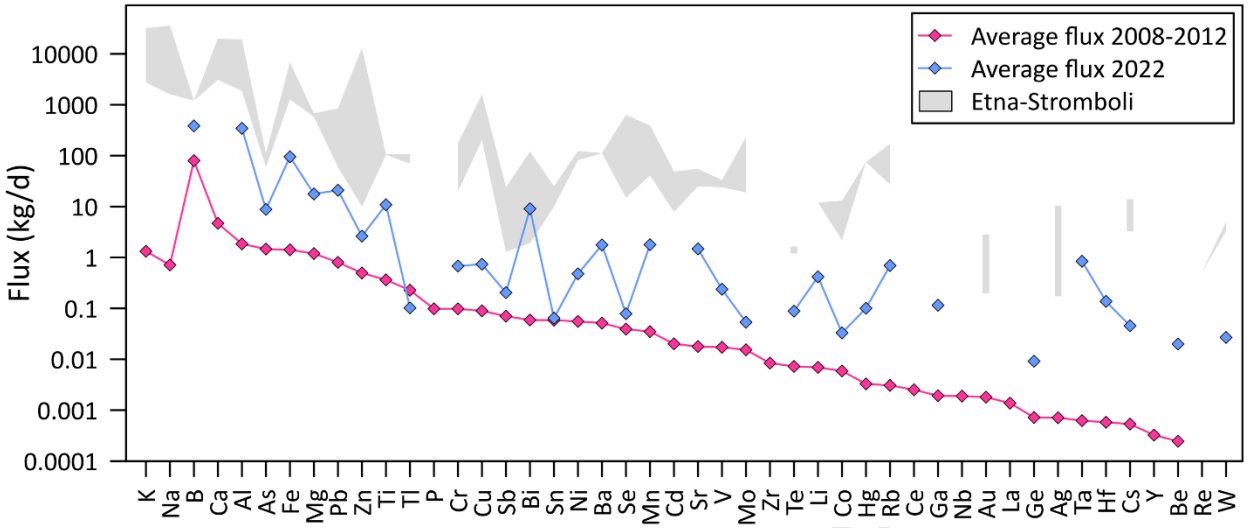

Fig. 10. Trace element emission rates from Vulcano in kg/d. Average fluxes for 2008-2012 and 2022. The grey shaded area delineates the emission rates from Etna and Stromboli (Buat-Ménard and Arnold, 1978, Bergametti et al., 1984, Andres et al., 1993, Gauthier and Le Cloarec, 1998, Allard et al., 2000, Calabrese et al., 2011, Calabrese et al., 2015).

Table 1 The chemical compostion of major and trace elements in fumarole vapor emissions from Vulcano, Italy

Fumarole	FA		F2	F5	F5	F4	F6	F11	F110	F12	F0	F0	F2	F2	F3	F3	F5	F5	F11	FZ	F0	FNB	FCB	FN3	F27	F202
Sample#	08-IT165	08-IT175	08-IT145	08-IT155	08-IT18a/b	09-IT035	09-IT045	09-IT01a/b	09-IT02B5	09-IT05a/b	12-VUL4	12-VUL5	12-VUL2	12-VUL9	12-VUL3	12-VUL6	12-VUL7	12-VUL-8	12-VUL1							
Date	12/08	13/08	11/08	11/08	5/13/08	14/09	14/09	15/09	12/09	15/09	4/13/12	13/12	4/12/12	14/12	12/12	4/13/12	4/14/12	4/14/12	4/12/12	2/12/22	2/11/22	2/12/22	2/12/22	2/12/22	2/12/22	2/12/22
T (°C)	328	230	251	407	397	382	115	272	253	412	363	363	296	296	322	322	398	398	228	94	361	359	284	244	97	234
Type sample	Cond.	Cond.	Cond.	Cond.	Cond.	Trap	Trap	Trap	Trap	Trap	NH4OH Trap	NH4OH	NH4OH Trap	NH4OH	NH4OH Trap	NH4OH Trap	NH4OH Trap	NH4OH Trap	NH4OH Trap	Cond.	Cond.	Cond.	Cond.	Cond.	Cond.	Cond.
Major elements (µmol/mol)																										
H_2O	884062000001	904052000001	914082000001	904052000001	903600	922548435	922548435	928200	973057330	930950	873800	873800	925000	921570000	915800	904400	904400	930700	921570000	824375600011	844076600011	845466600011	856336600011	866586600011	856336600011	885826600011
CO_2	019538100000	089538100000	078538100000	089538100000	85040	664184000	664184000	63489	545184000	55040	124100	124100	64500	645000	651050	831070	831070	60400	645000	756000000000	563000000000	363000000000	693000000000	983000000000	593000000000	594000000000
SO_2	952640000	922640000	942640000	902640000	3075	363500	363500	2430	902400	3355	225 0	225 0	232 0	232 0	264 0	324 0	324 0	225 0	232 0	420000	205000	056000	654000	543000	654000	540000
H_2S	938271	891750	613067	930071	1390	671760	671760	623	973034	97	880	880	1550	1550	1760	2160	2160	1330	1550	611	951	560	560	880	850	420
HCl	1621	1716	1611	1611	4195	2625	2625	3185	3518	8080	4160	4160	4260	4260	3620	6650	6650	3230	4260	2111	1151	1151	1451	5540	3361	3454
HF	103	163	133	185	61	250	250		185	500	35	35	150	155	25	23	23	155	155	112	132	338	418	859	349	

	8		8								1								0																
NH_3																													97.5	63.5	40.9	99.0	31.7	52.5	11.3
He																													0.9	1.1	0.8	0.6	0.6	1.4	1.3
H_2	57	58	95	156	nd		145	1740	930		80	378		33		33	370		370	145	145		720		720		745		9	23	16	15	6	81	75
N_2	2030	1985	1920	1830	1590		145	1740	930		80	378		1105		1105	980		980	135	135		1610		1610		650		748	562	623	911	885	388	456
CH_4	nd	nd	nd	nd	nd		nd	nd	nd		nd	nd		nd		nd	600		600	45	45		nd		nd		650		0.29	0.18	0.15	0.23	0.24	0.21	0.15
CO																													0.05	0.26	0.11	0.12	0.086	2.6	1.2
Trace elements (nmol/mol)																																			
Li	3.7	8.9	9.0	12	14	32	38	35	12	18	11	12	14	27		59			3.9				4.9	7.2	9.7	4.0		8.2		90	526	256	30		36
Na																	2128		177	1436			547		749		1225								
K														24	292		110	386	6.9	55		1879	3830	271		471	116	362							
Rb	0.02	1.6	0.3	0.3	0.5	3.0	1.0	0.3	0.2	0.2	0.2	0.7	0.5	0.04	0.3	0.7	0.1	0.3	0.1	0.09	0.06	0.2	0.2	1.1	0.05	0.4	0.1	0.3	0.1	1.4	7.4	3.1	4.8		4.3
Cs	0.002	0.1	0.009	0.02	0.03	0.2	0.007	0.01	0.004	0.01	0.01	0.02	0.02		0.2	0.01	0.001	0.009	0.009	0.005	0.03	0.1	0.007	0.2	0.02	1.2	0.008	0.03	0.01	0.8	3.2	1.1	0.2		0.1
Be	0.03	0.6	0.2	0.2	0.2	0.8	1.8	0.5	0.2	1.3	0.3	0.6	0.5		0.08			0.05	0.3		0.09	0.10		0.2	0.04	0.1		0.06	0.04	4.8	22	7.1	1.1	0.03	0.5
Mg	762	592	721	893	575	1730	1909	852	69	498	2615	690	391		270			137	8.7	27		170		55		34	132	828		1184	8588	1419	110		233
Ca	1140	883	1323	1286	963	2482	3469	2777	569	1414	5664	2340	3926	66	997	1083	276	482	154	302	71	508		161	31	241	606	2148							
Sr	0.3	0.6	1.3	1.0	1.2	1.6	11	3.9	0.8	1.8	12	3.1	1.9	1.0	8.3	1.5	0.6	1.0	0.7	0.4	0.2	1.1	0.2	1.8	0.2	1.2	1.5	4.9	0.7	24	181	49	7.0	0.3	5.4
Ba	0.2	1.9	2.1	2.6	8.0	21	9.4	2.6	0.9	3.0	2.9	4.1	2.2	9.5	25			0.6	6.0	7.3		13		16		8.7		10	0.4	23	1.6	6.2	148	1.3	14
Sc															0.0		0.0	0.0	0.0			0.0		0.0		0.0		0.2							

															5		0	6	1			0		5		1									
																	2					6													
																1																2			
	2			7	4							3		8		6	4				1	1		3						3	4	5	1		
T	.	5	1	.	.	7	2		1	2	1	3	6	5	5	8	.	1	5		.	3		.	3	8	5	9	1	8	4	0	3		8
i	1	5	0	5	7	9	2		0	1	8	8	8	4	2	2	7	6	4		1	8		8	4	6	6	7	0	8	3	4	5		6
	0	0	1	0		0				0	8	2	1	0	0			0		0		0		0		0		1	1			5	2		1
	.	.	.	.	3	.	1	1	1	.	.	.	.	.	.			.		.		.		.		.		.	.	1	5	.	.		.
V	1	2	1	5	4	8	7	2	2	9	2	1	3	3	5			7		2		2		4		3		7	4	2	4	6	1		0
	7	2																4	7			4				8			2					5	
C	.	.	1	8		8	9	4	1	3	2	4	2	4				.	.	2		.		1		.		2	1	1	6	1	9	.	1
r	2	9	1	7		1	6	1	8	0	9	1	8	9				7	7	3		2		2		5		9	2	6	4	3	2	3	4
	0	3	2	8				6	3	3	6	4	3		6			5						7		0					3	1		0	
M	.	.	.	.		1	1	.	.	.	.	.	.	5	.	7		.	1	3	1			.		.		1	2	4	3	0	1	.	1
n	4	6	1	5		5	1	9	3	4	1	1	8	3	0	5		4	7	6	2			2		4		2	7	3	6	5	9	5	1
																															1				
							1		1																				1	2	8	4			
		2	1	3		7	3	7	0	3	6	4	4	1						1								4	0	5	8	2	6		5
F	4	0	4	4		1	9	1	1	1	8	7	2	0				1	5	8				3		1		9	1	9	2	8	5	3	8
e	6	0	2	1		2	5	8	1	5	3	5	4	5				0	5	4				4		3		5	4	7	6	0	0	0	3
	0	0																																	
	.	.	0	0		0	5	9	2	0	3	1	1		0			0	0	0		1		0		0		0	2	0	6	1	0	0	0
C	0	0	.	.		.	.	.	.	.	.	.	.		.			.	.	.		.		.		.		.	.	.	.	.	.	.	.
o	4	8	1	2		5	9	0	3	9	1	7	3		3			8	1	1		0		5		4		9	6	7	1	0	9	0	2
	1	0	6						6						8			1		9				7		6			1	9				3	8
N	.	.	.	1		1	5	4	.	2		2	3		.			.	1	.		2		.		.		2	3	.	3	1	5	.	.
i	0	9	2	4		4	9	3	0	8		6	3		0			2	0	0		6		7		5		2	9	8	6	3	6	4	7
	0	3	1	5	6	3	1	1	3	9			9		2				2	1				0		5	0	4		8			3	1	3
C	.	.	.	.	.	.	6	2	.	.	2	1	.		.			1	.	.		3		.		.	.	.	1	.	8	8	.	.	.
u	6	3	4	4	4	0	2	0	1	5	1	2	1		3			7	5	2		4		9		2	9	9	6	5	6	2	8	7	1
							2				2	1			5			1			4	2	2		8	1		1			5				
Z	3	1	9	9	3	8	6	8	3	7	7	0	9	1	2	9	1	2	1	1	.	1	6	2	.	1	2	3	2	2	0	4	1	2	2
n	7	3	3	7	1	3	6	8	8	3	8	4	9	3	7	5	2	5	9	1	3	7	3	6	2	3	7	6	3	8	1	8	9	2	8
	0	5	1	0	0	7	0	0	1	0	0	2	2	0	0	0	0	0	0	0	0	0	0	3	0	1	0	0							
Z	.	.	.	.	.	.	.	.	.	.	.	.	.	.	.	.	.	.	.	.	.	.	.	.	.	.	.	.							
r	4	7	2	8	4	0	4	5	3	4	6	4	3	3	4	8	5	5	2	3	1	1	1	0	2	3	4	8							
	0		0				0							0	0			0	0	0		0		0		0									
	.	1	.	0	0	2	.	0	0	0	0	0	0	.	.			.	.	.		.		.		.		0							
N	0	.	0	.	.	.	0	.	.	.	.	.	.	0	0			0	0	0		0		0		0		.							
b	5	4	7	1	2	6	8	1	1	1	1	3	7	8	1			1	1	2		1		8		7		1							
	0	0	0	0	1	2	4	3	3	0	2	0	0		0				8	7				2		2			1	0	1	5	0	0	0
M	.	.	.	.	.	.	.	.	.	.	.	.	.		.				.	.		3		.		.			.	.	.	.	.	.	.
o	5	5	1	5	9	5	3	3	4	3	2	7	4		3				1	2		2		2		8			2	9	2	3	8	2	4
		0																0		0		0	0	0	0			0							
		.		0			0	0	0	0	0	0	0		0	0		.		.		.	.	.	.		0	.							
		0		.	0	0	.	.	.	.	.	.	.		.	.		0		0		0	0	0	0		.	0							
R		0		0	.	.	0	0	0	0	0	0	0		0	0		0		0		0	0	0	0		0	0							
u		9		1	3	1	4	4	4	1	2	2	1		1	4		3		4		1	1	1	1		2	3							
			0	0																															
			.	.	0	0	0	0	0	0	0	0	0																						
			0	0	.	.	.	.	.	.	.	.	.																						
R			0	0	0	0	0	0	0	0	0	0	0																						
h			1	4	1	1	3	4	2	2	5	4	3																						
	0	0	0	0	0	0	0	0	0	0	0	0	0																						
	.	.	.	.	.	.	.	.	.	.	.	.	.																						
P	0	0	0	0	0	0	0	0	0	0	0	0	2																						
d	5	6	6	4	3	3	8	8	2	4	6	9	1																						
																						0				0									
	0	0	0	0	0	0		0	0		0	0			0			0	0	0	0	.	0		0	.	0	0							
	.	.	.	.	.	.	0	.	.	0	.	.	0	0	.	0		.	.	.	.	0	.	0	.	0	.	.							
A	0	0	0	0	0	0	.	0	0	.	0	0	.	.	0	.		0	0	0	0	0	0	.	0	0	0	0							
g	2	5	5	4	1	2	6	3	6	2	5	3	1	2	4	3		9	4	3	8	2	1	2	1	3	5	9							
																					0														
	0																0		0		.		0	0	0		0								
	.	0	0	0	8	3			3	0	2	4	1		0	0	.	0	.		0	0	.	.	.	0	.	0							
C	0	.	.	.	.	.	1	1	.	.	.	.	.		.	.	0	.	0		0	.	0	0	0	.	0	.							
d	2	3	1	2	5	4	4	0	0	5	9	8	5		1	2	2	2	6		5	4	4	3	4	1	7	2							
									0	0	0	0	0											0		0			0	0	0		0	0	0
H									.	.	.	.	.											.		.			.	.	.	1	.	.	.
f									2	0	0	1	3											0		0			0	4	8	0	5	0	2

Ta	0.1	0.1	0.03	0.04	0.01	0.04	0.03	0.03	0.1	1 0.03	1 0.04	0.1	0.3					0.002						4 0.01		04 0.01		0.005	1 0.1	9.9	1.1	12	47	1	2.4
W																													0.2	0.8	0.4	0.4	0.5	0.1	0.2
Re															0.0003		0.0001	0.0002	0.0002	0.0003		0.0003				0.00003									
Ir								0.01	0.01		0.01	0.01	0.01																						
Pt	0.0003	0.003	0.0008	0.0005	0.0008	0.002	0.006	0.004	0.01	0.003	0.004	0.007	0.005		0.003		0.00005	0.002		0.00003		0.0009		0.0006		0.0005	0.002	0.0006							
Au	0.03	0.06	0.03	0.03	0.01	0.02	0.6	0.3	0.1	0.2	0.3	0.3	0.5	0.02	0.004	0.05	0.007	0.008	0.004	0.005	0.006		0.008		0.005	0.001	0.01	0.001							
Hg														0.1		0.5	0.4	0.04	0.04	0.06	0.07	0.2	0.7	0.08	0.4	0.02	0.8		0.3	0.8	0.7	3.1	2.2	0.2	0.7
Al	1545	1944	2227	2098	1504	4154	2102	458	311	399	902	485	432	39	170	274	82	411	106	49	70	15	30	514	37	106	2	535	487	2815	14069	3018	2873		2480
Ga	0.03	0.3	0.2	0.07	3.0	2.7	0.3	0.02	0.08	0.3	0.1	0.05	0.1	0.01	0.1		0.04	0.1	0.01	0.04	0.004	0.02	0.01	0.1	0.01	0.1	0.04	1.0	0.1	3.1	1.8	4.1	0.8		0.4
Tl	2.3	0.8	20	12	22	139	8.5	0.4	0.1	4.9	2.6	65	50	1.8	0.5	2.2	3.0	0.6	1.9	1.9	6.0	0.3	3.1	0.5	4.1	0.03	0.4	3.5	0.02	1.2	5.6	0.04	0.02		0.7
Sn	0.7	11	2.6	3.7	1.6	79	6.9	0.7	0.4	1.3	1.3	4.2	8.6	2.1	12	3.6	0.3	11	0.04	0.05	0.1	1.3	0.3	0.4	0.1	1.1	1.6	13	0.09	1.9	2.4	3.0	0.8	0.08	0.4
Pb	1.2	6.9	3.7	35	139	423	31	6.2	0.6	32	23	237	200	2.8	3.0	6.4	13	3.7	24	2.5	24	0.7	7.7	0.1	7.0	0.3	9.8	4.1	3.5	315	1306	6.0	3.6	0.1	5.4
Bi	1.1	2.2	11	1.1	1.4	3.7	3.6	0.7	0.1	0.4	0.3	3.1	16	0.5	0.4	0.9	0.8	0.3	1.7	0.2	0.9	0.001	1.7	0.01	1.7		0.5	0.02	5.5	74	623	1.3	0.5	0.2	0.5
B	17213	11712	18068	19495	85008	97746	17056	26005	26738	13045	44129	72163	16446	5912	20226	11653	16888	11258	9980	13831	7434	15666	10124	19031	12882	10281	11252	88580	809	65504	76985	73006	30075	555	29271

	1	9	9	2			1	8		9			1		8			2				3		5		7							5		
Si														617	135034	1884	4770	28938	17458	4294	2574	26926	14715	43913	5676	50310	19998	177914							
Ge		0.1			0.08	0.3									0.5			0.5	0.3		0.1	0.7		0.1		0.5	0.01	0.2	0.07	0.2	1.2	0.3	0.2		0.04
As	306	333	1494	139	11	55	96	26	81	159	108	104	418	510	1013	273	73	349	48	55	37	324	33	183	43	259	77	1062	9	221	417	216	760	4.7	154
Sb	37	24	14	38	10	11	6.5	0.6	5.3	0.9	0.7	0.3	2.0	1.7	18	3.9	1.2	5.7	0.7	0.8	0.7	5.1	0.6	4.8	0.7	2.5	1.1	4.3	3.0	3.4	2.6	4.8	11	0.3	3.0
Te														0.4	2.4	0.5	0.3	1.0	0.4	0.7	0.5	0.9	0.6	0.5	0.7	1.1	1.3	0.03	0.4	2.9	2.2	2.1	2.8	0.2	0.7
P	13	14	28	24	15	29	129	46	36	80	43	56	48		57	75	1.7	54	1.4	6.4	2.1	39	4.3	18		15	24	336							
Se	16						15	4.0	1.6	1.0	1.6	4.1	2.3	6.6	35	5.3	1.2	20	2.8	0.6	2.7	84	1.8	3.1	3.0	47	2.6	0.1	0.6	9.5	4.9	0.6	1.5	0.7	
Y	0.007	0.1	0.05	0.03	0.08	0.3	0.04	0.05	0.02	0.04	0.1	0.05	0.04		0.03	0.01	0.01	0.03	0.01	0.01		0.01	0.01	0.1	0.004	0.04	0.004	0.05							
La	0.03	0.1	0.1	0.1	0.3	0.8	0.08	0.1	0.05	0.08	0.4	0.09	0.06	0.02	0.07	0.04	0.06	0.09	0.02		0.001	0.01	0.07	0.004	0.05	0.09	0.08	0.09							
Ce	0.06	0.3	0.2	0.2	0.4	1.3	0.1	0.2	0.09	0.1	0.6	0.2	0.09	0.03	0.07	1.8	0.08	0.07	0.03	0.02	0.001	0.003	0.02	0.01	0.001	0.1	0.02	0.07							
Pr							0.01	0.02	0.01	0.01	0.06	0.02	0.003		0.01		0.01	0.01	0.004	0.003	0.003	0.001	0.0002	0.001	0.001	0.01	0.002	0.01							
Nd							0.03	0.05	0.03	0.05	0.2	0.05	0.03		0.02	0.02	0.02	0.03	0.02	0.004		0.01	0.04	0.02		0.04	0.02	0.05							
Sm											0.03				0.001			0.01	0.003			0.002		0.001		0.004		0.01							
Eu											0.003				0.002			0.001							0.004	0.001		0.002							
Gd									0.004	0.01	0.03			0.001	0.001		0.005	0.003		0.001		0.000	0.003	0.001	0.002	0.004	0.001	0.01							

																					2							
Tb														0.0003			0.0004	0.0004				0.0001			0.0003		0.002
Dy														0.005	0.01	0.001	0.003	0.001	0.003	0.0001			0.002		0.003		0.005
Ho							0.01	0.01	0.02	0.004	0.01	0.01			0.001	0.002	0.0002	0.001	0.0002	0.001	0.0002	0.0002	0.0002	0.001		0.0004	0.001	0.001
Er							0.001			0.001	0.01	0.001						0.002	0.002	0.001	0.00001	0.00004	0.0002	0.002		0.001		0.004
Tm														0.001			0.0004	0.00002		0.0005		0.0001		0.0003		0.0003		0.001
Yb															0.002		0.0001	0.001	0.001			0.0001	0.001	0.002		0.003	0.001	0.003
Lu															0.0002	0.001		0.0002					0.0004	0.001		0.0004		0.001
Th	0.002	0.09	0.02	0.03	0.1	0.4	0.02	0.09	0.06	0.01	0.07	0.1	0.02		0.02		0.01	0.009	0.004	0.0002		0.0002	0.002	0.005	0.001	0.03	0.001	0.004
U	0.001	0.04	0.006	0.007	0.009	0.09	0.02	0.01	0.001	0.02	0.03	0.01	0.004	0.002	0.009	0.004	0.003	0.003	0.003	0.0002	0.0003	0.002	0.001	0.03	0.001	0.01	0.004	0.01

Table 2
Dominant gaseous compound predicted from thermodynamic calculations

	300°C	600°C	1000 °C
Alkali metals			
Li	LiCl, $LiAlF_4$	LiCl	LiCl, LiOH
Na	NaCl, NaF	NaCl	NaCl
K	KF, KCl	KCl, KF	KCl
Rb	RbCl	RbCl	RbCl
Cs	CsCl	CsCl	CsCl
Alkaline earth metals			
Be	$Be(OH)_2$	$Be(OH)_2$	$Be(OH)_2$

Mg	$MgCl_2$	$MgCl_2$, $Mg(OH)_2$	$Mg(OH)_2$, $MgCl_2$
Ca	$CaCl_2$	$CaCl_2$	$CaCl(OH)$, $CaCl_2$, $Ca(OH)_2$
Sr	$SrCl_2$	$SrCl_2$	$SrCl(OH)$, $SrCl_2$
Ba	$BaCl_2$	$BaCl_2$	$BaCl_2$, $BaCl(OH)$
Transition metals			
Ti	$TiOCl_4$	$TiOCl_2$	$TiOCl_2$
V	$VOCl_2$, $VOCl_3$	$VOCl_2$	$VOCl$, $VOCl_2$
Cr	$CrCl_3$	$Cr(OH)_3$, $CrCl_3$	$Cr(OH)_3$
Mn	$MnCl_2$	$MnCl_2$	$MnCl_2$
Fe	$FeCl_2$	$FeCl_2$, $Fe(OH)_2$	$Fe(OH)_2$, $FeCl_2$
Co	$CoCl_2$	$CoCl_2$, $Co(OH)_2$	$Co(OH)_2$, $CoCl_2$
Ni	$NiCl_2$	$NiCl_2$, $Ni(OH)_2$	$Ni(OH)_2$, $NiCl_2$
Cu	$CuCl$	$CuCl$	$CuCl$
Zn	$ZnCl_2$	$ZnCl_2$	$ZnCl_2$, $Zn(OH)_2$, Zn
Zr	ZrF_4	ZrF_4, $ZrCl_4$	$ZrCl_4$, ZrF_4
Nb	$NbOF_3$, $NbOCl_3$	$NbOF_3$, $NbOCl_3$	$NbOCl_3$, $NbOF_3$
Mo	MoO_2F_2	MoO_2F_2	$MoO_2(OH)_2$, MoO_2F_2
Ag	$AgCl$	$AgCl$	$AgCl$, Ag
Cd	$CdCl_2$, $Cd(OH)_2$	Cd, $Cd(OH)_2$	$Cd(OH)_2$, Cd
W	$WO_2(OH)_2$, WO_2Cl_2	$WO_2(OH)_2$	$WO_2(OH)_2$
Re	$ReCl_3$	$ReCl_3$, ReO_3	ReO_3, $ReCl_3$
Au	AuS	AuS	AuS
Hg	Hg	Hg	Hg
Post-transition metals			
Al	$Al(OH)_3$, $AlF(OH)_2$	$Al(OH)_3$	$Al(OH)_3$
Ga	$GaCl_3$	$GaCl$, $GaCl_3$	$GaCl$
Tl	TlO	TlO	TlO
Sn	$SnCl_2$	SnS, $SnCl_2$	SnS, $SnCl_2$
Pb	$PbCl_2$	PbS, $PbCl_2$	PbS, $PbCl$, $PbCl_2$
Bi	$BiCl_3$	BiS, Bi	BiS, Bi, $BiCl$, $BiCl_2$
B	$B(OH)_3$	$B(OH)_3$	$B(OH)_3$
Metalloids and non-metals			
Si	$Si(OH)_4$	$Si(OH)_4$	$Si(OH)_4$
Ge	$GeCl_4$, GeS	GeS, GeO	GeS, GeO
As	As_2S_3	As_2S_3, AsS, As_2	AsS, As_2, AsO
Sb	$SbCl$, $SbCl_3$	$SbCl$	$SbCl$
Te	TeS, $TeCl_2$	TeS	TeS, TeH, Te
P	H_3PO_4	H_3PO_4	H_3PO_4
Se	SeH_2, SeS, Se_2	SeH_2, SeS	SeH_2, SeS

Table 3
Gas-solid reactions

	Gas-solid reaction	Mineral formation temperature
Alkali metals		
Li	$2LiCl(g) + SO_2(g) + 2H_2O(g) = Li_2SO_4(s) + 2HCl(g) + H_2(g)$	100-500°C
Na	$2NaCl(g) + SO_2(g) + 2H_2O(g) = K_2SO_4(s) + 2HCl(g) + H_2(g)$	100-200°C
	$NaCl(g) + Al(OH)_3(g) + 3Si(OH)_4(g) = NaAlSi_3O_8(s) + HCl(g) + 7H_2O(g)$	200-900°C
K	$2KCl(g) + SO_2(g) + 2H_2O(g) = K_2SO_4(s) + 2HCl(g) + H_2(g)$	100-200°C
	$KCl(g) + Al(OH)_3(g) + 3Si(OH)_4(g) = KAlSi_3O_8(s) + HCl(g) + 7H_2O(g)$	200-750°C
Rb	$2RbCl(g) + SO_2(g) + 2H_2O(g) = Rb_2SO_4(s) + 2HCl(g) + H_2O(g)$	100-200°C
	$RbCl(g) = RbCl(s)$	200-400°C
Cs	$CsCl(g) + Al(OH)_3(g) + 2SO_2(g) + H_2O(g) = CsAl(SO_4)_2(s) + HCl(g) + 2H_2(g)$	100-250°C
	$CsPO_3(g) = CsPO_3(s)$	280-320°C
	$CsCl(g) + Al(OH)_3(g) + Si(OH)_4 = CsAlSiO_4(s) + 3H_2O(g) + HCl(g)$	400-550°C
Alkaline earth metals		

Be	$Be(OH)_{2(g)} + SO_2(g) = BeSO_4(s) + H_2(g)$	100°C
	$3Be(OH)_2(g) + 2Al(OH)_3(g) + 6Si(OH)_4(g) = Be_3Al_2Si_6O_{18}(s) + 18H_2O(g)$	150-800°C
Mg	$MgCl_2(g) + SO_2(g) + 2H_2O(g) = MgSO_4(s) + 2HCl(g) + H_2(g)$	100-250°C
	$MgCl_2(g) + Si(OH)_4(g) = MgSiO_3(s) + 2HCl(g) + H_2O(g)$	250-700°C
	$Mg(OH)_2(g) + Si(OH)_4(g) = MgSiO_3(s) + 3H_2O(g)$	700-900°C
Ca	$CaCl_2(g) + 2Al(OH)_3(g) + 2Si(OH)_4(g) = CaAl_2Si_2O_8(s) + 2HCl(g) + 6H_2O(g)$	250-1000°C
	$CaCl_2(g) + SO_2(g) + 2H_2O(g) = CaSO_4(g) + 2HCl(g) + H_2(g)$	100-250°C
Sr	$SrCl_2(g) + 2Al(OH)_3(g) + 2Si(OH)_4(g) = SrAl_2Si_2O_8(s) + 2HCl(g) + 6H_2O(g)$	250-1000°C
	$SrCl_2(g) + SO_2(g) + 2H_2O(g) = SrSO_4(g) + 2HCl(g) + H_2(g)$	100-250°C
Ba	$BaCl_2(g) + 2Al(OH)_3(g) + 2Si(OH)_4(g) = BaAl_2Si_2O_8(s) + 2HCl(g) + 6H_2O(g)$	300-900°C
	$BaCl_2(g) + SO_2(g) + 2H_2O(g) = BaSO_4(g) + 2HCl(g) + H_2(g)$	100-300°C
Transition metals		
Ti	$TiOCl_2(g) + H_2O(g) = TiO_2(s) + 2HCl(g)$	100-1000°C
V	$2VOCl_2(g) + {}^3/_2O_2(g) + 4H_2(g) = V_2O_3(s) + 4HCl(g) + 2H_2O(g)$	300-950°C
	$2VOCl_3(g) + {}^3/_2O_2(g) + 5H_2(g) = V_2O_3(s) + 6HCl(g) + 2H_2O(g)$	100-300°C
Cr	$Cr(OH)_3(g) = CrO_2(s) + H_2O(g) + {}^1/_2H_2(g)$	700-850°C
	$Cr(OH)_3(g) + HCl(g) = CrClO(s) + 2H_2O(g)$	550-700°C
	$CrCl_3(g) + H_2O(g) = CrClO(s) + 2HCl(g)$	100-550°C
Mn	$MnCl_2(g) + Si(OH)_4(g) = MnSiO_3(s) + 2HCl(g) + H_2O(g)$	300-850°C
	$MnCl_2(s) + SO_2(g) + 2H_2O(g) = MnSO_4(s) + 2HCl(g) + H_2(g)$	100-300°C
Fe	$3Fe(OH)_2(g) = Fe_3O_4(s) + 2H_2O(g) + H_2(g)$	700-1000°C
	$3FeCl_2(g) + 4H_2O(g) = Fe_3O_4(s) + 6HCl(g) + H_2(g)$	450-700°C
	$FeCl_2(g) + 2H_2S(g) = FeS_2(s) + 2HCl(g) + H_2(g)$	250-400°C
	$CuCl(g) + FeCl_2(g) + 2H_2S(g) = CuFeS_2(s) + 3HCl(g) + {}^1/_2H_2(g)$	300-600°C
	$FeCl_2(g) + SO_2(g) + 2H_2O(g) = FeSO_4(s) + 2HCl(g) + H_2(g)$	100-250°C
Co	$CoCl_2(g) + H_2S(g) = CoS(s) + 2HCl(g)$	550-750°C
	$CoCl_2(g) + 2H_2S(g) = CoS_2(g) + 2HCl(g) + H_2(g)$	100-550°C
Ni	$Ni(OH)_2(g) + H_2S(g) = NiS(s) + 2H_2O(g)$	800-950°C
	$NiCl_2(g) + H_2S(g) = NiS(s) + 2HCl(g)$	450-800°C
	$NiCl_2(g) + 2H_2S(g) = NiS_2(s) + 2HCl(g) + H_2(g)$	100-450°C
Cu	$2CuCl(g) + 2H_2S(g) = Cu_2S(s) + 2HCl(g)$	600-1000°C
	$CuCl(g) + FeCl_2(g) + 2H_2S(g) = CuFeS_2(s) + 3HCl(g) + {}^1/_2H_2(g)$	300-600°C
	$6CuCl(g) + As_2S_3(g) + 5H_2S(g) = 2Cu_3AsS_4(s) + 6HCl(g) + 2H_2(g)$	100-300°C
Zn	$ZnCl_2(g) + H_2S(g) = ZnS(s) + HCl(g)$	100-700°C
	$ZnCl_2(g) + SO_2(g) + 2H_2O(g) = ZnSO_4(s) + 2HCl(g) + H_2(g)$	100°C
Zr	$ZrCl_4(g) + 4H_2O(g) = Zr(OH)_4(s) + 4HCl$	100°C
	$ZrCl_4(g) + Si(OH)_4(g) = ZrSiO_4(s) + 4HCl(g)$	100-700°C
Nb	$2NbOCl_3(g) + 3H_2O(g) = Nb_2O_5(s) + 3HCl(g)$	100-1000°C
Mo	$MoF_2O_2(g) + 2H_2S(g) + H_2(g) = MoS_2(s) + 2HF(g) + 2H_2O(g)$	100-250°C
Ag	$2AgCl(g) + H_2S(g) = Ag_2S(s) + 2HCl(g)$	100-500°C
Cd	$CdCl_2(g) + 2H_2S(g) = CdS_2(s) + 2HCl(g) + H_2(g)$	100-500°C
W	$WH_2O_4(g) = WO_3(s) + H_2O(g)$	150-400°C
	$WO_2Cl_2(g)\ 2H_2O(g) = H_2WO_4(s) + 2HCl(g)$	100°C
Re	$ReCl_3(g) + 2H_2S(g) = ReS_2(s) + 3HCl(g) + {}^1/_2H_2(g)$	300-750°C
	$2ReCl_3(g) + 7H_2S(g) = Re_2S_7(s) + 6HCl(g) + 4H_2(g)$	300°C
Au	$AuS(g) + H_2(g) = Au(s) + H_2S(g)$	250-450°C
	$AuS(g) + SeH_2(g) = AuSe(s) + H_2S(g)$	100-250°C
Hg	$Hg(g) + 2HS_2S(g) = HgS(s) + H_2(g)$	100-150°C

Post-transition metals		
Al	$NaCl(g) + Al(OH)_3(g) + 3Si(OH)_4(g) = NaAlSi_3O_8(s) + HCl(g) + 7H_2O(g)$	200-900°C
	$KCl(g) + Al(OH)_3(g) + 3Si(OH)_4(g) = KAlSi_3O_8(s) + HCl(g) + 7H_2O(g)$	200-750°C
	$CaCl_2(g) + 2Al(OH)_3(g) + 2Si(OH)_4(g) = CaAl_2Si_2O_8(s) + 2HCl(g) + 6H_2O(g)$	250-1000°C
	$Al(OH)_3(g) + 3HF(g) = AlF_3(s) + 3H_2O(g)$	100-500°C
Ga	$2GaCl(g) + 3H_2O(g) = Ga_2O_3(s) + 2HCl(g) + 2H_2(g)$	550-750°C
	$2GaCl_3(g) + 3H_2O(g) = Ga_2O_3(s) + 6HCl(g)$	400-550°C
	$2GaCl_3(g) + 3H_2S(g) = Ga_2S_3(s) + 6HCl(g)$	100-400°C
Tl	No mineral formed	
Sn	$SnCl_2(g) + 2H_2O(g) = SnO_2(g) + 2HCl(g) + H_2(g)$	400-550°C
	$SnCl_2(g) + SO_2(g) + 2H_2O(g) = SnSO_4(s) = 2HCl(g) + H_2(g)$	100-450°C
Pb	$PbCl_2(g) + H_2S(g) = PbS(s) + HCl(g)$	250-500°C
	$PbCl_2(g) + SO_2(g) + 2H_2O(g) = PbSO_4(s) + 2HCl(g) + H_2(g)$	100-250°C
Bi	$2BiS(g) + H_2S(g) = Bi_2S_3(s) + H_2(g)$	400-500°C
	$2BiCl_3(g) + 3H_2S(g) = Bi_2S_3(s) + 6HCl(g)$	250-400°C
	$2BiCl_3(g) + 2SO_2(g) + 4H_2O(g) = Bi_2(SO_4)_2(s) + 6HCl(g) + H_2(g)$	100-250°C
B	No mineral formed	
Metalloids and non-metals		
Si	$Si(OH)_4(g) = SiO_2(s) + 2H_2O(g)$	100-850°C
Ge	$GeS(g) + 2H_2O(g) = GeO_2(s) + H_2S(g) + H_2(g)$	350-450°C
	$GeCl_4(g) + 2H_2O(g) = GeO_2(s) + 4HCl(g)$	100-350°C
As	$6CuCl(g) + As_2S_3(g) + 5H_2S(g) = 2Cu_3AsS_4(s) + 6HCl(g) + 2H_2(g)$	100-300°C
	$As_2S_3(g) = As_2S_3(s)$	100-150°C
Sb	No mineral formed	
Te	$TeCl_2(g) + H_2O(g) = TeO(s) + 2HCl(g)$	100-250°C
P	$H_3PO_4(g) = H_3PO_4(s)$	100-200°C
Se	$SeH_2(g) = Se(s) + H_2(g)$	100-150°C
	$AuS(g) + SeH_2(g) = AuSe(s) + H_2S(g)$	100-250°C

Table 4
Trace element emission rates from Vulcano, Stromboli and Etna (Italy) in kg/day unless specified otherwise.

	Vulcano				Stromboli*	Etna*
	2008-2012			2022		
SO_2 (t/d)	12	±	1	79	300	1000-4560
Alkali metals						
Li	0.007	±	0.003	0.4	12	
Na	0.7	±			1616	26000-36000
K	1.3	±			2740	5992-32000
Rb	0.003	±	0.002	0.7	27	74-170
Cs	0.001	±	0.0005	0.05	4.1	3.8-12
Alkaline earth metals						
Be	0.0002	±	0.0002	0.02		
Mg	1.2	±	0.9	18		581-674
Ca	4.7	±	4.1			3090-20000
Sr	0.02	±	0.02	1.5		25-55
Ba	0.05	±	0.01	1.8		112

Transition metals						
Sc	0.0001	±				
Ti	0.4	±	0.4	11		104-107
V	0.02	±	0.02	0.2		24-33
Cr	0.10	±	0.06	0.7	164	20-173
Mn	0.03	±	0.03	1.8		41-390
Fe	1.4	±	1.6	95		1282-6700
Co	0.006	±	0.009	0.03	2.2	5.2-13
Ni	0.06	±	0.05	0.5	123	82-100
Cu	0.09	±	0.1	0.7	205	300-1600
Zn	0.5	±	0.2	2.6	356	10-13000
Zr	0.008	±	0.005			
Nb	0.002	±	0.002			
Mo	0.02	±	0.009	0.05		19-230
Ru	0.0002	±	0.0002			
Rh	0.0002	±	0.0002			
Pd	0.0005	±	0.0002			
Ag	0.001	±	0.001		0.2	4-9
Cd	0.02	±	0.02		15	7.9-49
Hf	0.001	±	0.001	0.1		
Ta	0.001	±	0.001	0.8		
W				0.03	3.3	5
Re	0.000001	±				0.52
Ir	0.0001	±				
Pt	0.00004	±	0.00004			
Au	0.002	±	0.003		0.5	0.23-2.4
Hg	0.003	±		0.1		75
Post-transition metals						
Al	1.8	±	1.7	345	1863	3556-19000
Ga	0.002	±	0.002	0.1		
Tl	0.2	±	0.2	0.1		70-107
Sn	0.06	±	0.05	0.06	10	15-25
Pb	0.8	±	0.6	21	96	60-850
Bi	0.06	±	0.06	9.1	10	1.9-120
B	80	±	27	384		1211
Metalloids and non-metals						
Si	77	±				
Ge	0.001	±	0.0005	0.01		
As	1.5	±	0.60	8.8	60	60-110
Sb	0.07	±	0.07	0.2	1.3	10-24
Te	0.007	±		0.09	1.4	
P	0.10	±	0.06			
Se	0.04	±	0.04	0.08	15	48-630

Rear Earth Elements and Actinites			
Y	0.0003	±	0.0002
La	0.001	±	0.001
Ce	0.003	±	0.001
Pr	0.0001	±	0.0001
Nd	0.0005	±	0.0004
Sm	0.00004	±	0.00003
Eu	0.00001	±	0.000001
Gd	0.0001	±	0.00004
Tb	0.000002	±	
Dy	0.00002	±	
Ho	0.0001	±	0.0001
Er	0.00002	±	0.00002
Tm	0.000002	±	
Yb	0.00001	±	
Lu	0.000002	±	
Th	0.001	±	0.001
U	0.0002	±	0.0001

*Data from Stromboli and Etna: Buat-Ménard and Arnold, 1978; Bergametti et al., 1984; Andres et al., 1993; Gauthier and Le Cloarec, 1998; Allard et al., 2000; Calabrese et al., 2011; Calabrese et al., 2015

Author statement

Celine L. Mandon: Conceptualization, Methodology, Software, Investigation, Visualization, Writing - original draft, Writing - review & editing. Hanna Kaasalainen: Conceptualization, Methodology, Formal analysis, Writing - review & editing. Sergio Calabrese: Methodology, Writing - review & editing. Everett L. Shock: Methodology, Writing - review & editing. Panjai Prapaipong: Methodology, Writing - review & editing. Franco Tassi: Methodology, Writing - review & editing. Ingvi Gunnarsson: Methodology. Jóhann Gunnarsson-Robin: Methodology, Writing - review & editing. Andri Stefánsson: Conceptualization, Methodology, Investigation, Formal analysis, Visualization, Writing - original draft, Writing - review & editing.

Declaration of interests

☒The authors declare that they have no known competing financial interests or personal relationships that could have appeared to influence the work reported in this paper.

☐The authors declare the following financial interests/personal relationships which may be considered as potential competing interests:

Highlights

- For most trace elements, a meaningful range of one order of magnitude is expected
- Improvement of thermodynamic data and models is needed for volcanic gas transport
- Dominant transport as chloride, hydroxide, and mixed hydroxy-chloro gas species
- Efficient precipitation of trace elements in the subsurface prevented by kinetics